



HAL
open science

Bacterial Lipopolysaccharides Exacerbate Neurogenic Heterotopic Ossification Development

Marjorie Salga, Selwin Gabriel Samuel, Hsu Wen Tseng, Laure Gatin, Dorothee Girard, Bastien Rival, Valérie Barbier, Kavita Bisht, Svetlana A. Shatunova, Charlotte Debaud, et al.

► **To cite this version:**

Marjorie Salga, Selwin Gabriel Samuel, Hsu Wen Tseng, Laure Gatin, Dorothee Girard, et al.. Bacterial Lipopolysaccharides Exacerbate Neurogenic Heterotopic Ossification Development. *Journal of Bone and Mineral Research*, 2023, 10.1002/jbmr.4905 . hal-04233256

HAL Id: hal-04233256

<https://hal.science/hal-04233256v1>

Submitted on 18 Oct 2023


HAL is a multi-disciplinary open access archive for the deposit and dissemination of scientific research documents, whether they are published or not. The documents may come from teaching and research institutions in France or abroad, or from public or private research centers.

L'archive ouverte pluridisciplinaire **HAL**, est destinée au dépôt et à la diffusion de documents scientifiques de niveau recherche, publiés ou non, émanant des établissements d'enseignement et de recherche français ou étrangers, des laboratoires publics ou privés.



Distributed under a Creative Commons Attribution - NonCommercial - NoDerivatives 4.0 International License

Bacterial Lipopolysaccharides Exacerbate Neurogenic Heterotopic Ossification Development

Marjorie Salga,^{1,2,3} Selwin G Samuel,^{1,4} Hsu-Wen Tseng,¹ Laure Gatin,^{2,3,5} Dorothée Girard,⁶ Bastien Rival,⁶ Valérie Barbier,¹ Kavita Bisht,¹ Svetlana Shatunova,¹ Charlotte Debaud,² Ingrid G Winkler,¹ Julie Paquereau,³ Aurélien Dinh,⁷ Guillaume Genêt,² Sébastien Kerever,⁸ Paer-Sélim Abback,⁹ Sébastien Banzet,⁶ François Genêt,^{2,3} Jean-Pierre Lévesque,¹ and Kylie A Alexander¹ 

¹Mater Research Institute—The University of Queensland, Translational Research Institute, Woolloongabba, Australia

²University of Versailles Saint Quentin en Yvelines, END:ICAP U1179 INSERM, UFR Simone Veil-Santé, Montigny le Bretonneux, France

³UPOH (Unité Péri Opératoire du Handicap), Physical and Rehabilitation Medicine Department, Raymond-Poincaré Hospital, Assistance Publique-Hôpitaux de Paris (AP-HP), Garches, France

⁴Department of Oral Pathology and Microbiology, Saveetha Dental College and Hospitals, Chennai, India

⁵Department of Orthopedic Surgery, Raymond Poincaré Hospital, AP-HP, Garches, France

⁶Institut de Recherche Biomédicale des Armées (IRBA), INSERM UMR-MD 1197, Clamart, France

⁷Department of Infectious Diseases, Raymond Poincaré Hospital, AP-HP, Garches, France

⁸Department of Anesthesiology and Critical Care, Lariboisière University Hospital, AP-HP, Paris, France

⁹Department of Anesthesiology and Critical Care, Beaujon Hospital, DMU Parabol, AP-HP, Clichy, France

ABSTRACT

Neurogenic heterotopic ossifications (NHO) are heterotopic bones that develop in periarticular muscles after severe central nervous system (CNS) injuries. Several retrospective studies have shown that NHO prevalence is higher in patients who suffer concomitant infections. However, it is unclear whether these infections directly contribute to NHO development or reflect the immunodepression observed in patients with CNS injury. Using our mouse model of NHO induced by spinal cord injury (SCI) between vertebrae T₁₁ to T₁₃, we demonstrate that lipopolysaccharides (LPS) from gram-negative bacteria exacerbate NHO development in a toll-like receptor-4 (TLR4)-dependent manner, signaling through the TIR-domain-containing adapter-inducing interferon- β (TRIF/TICAM1) adaptor rather than the myeloid differentiation primary response-88 (MYD88) adaptor. We find that T₁₁ to T₁₃ SCI did not significantly alter intestinal integrity nor cause intestinal bacteria translocation or endotoxemia, suggesting that NHO development is not driven by endotoxins from the gut in this model of SCI-induced NHO. Relevant to the human pathology, LPS increased expression of osteoblast markers in cultures of human fibro-adipogenic progenitors isolated from muscles surrounding NHO biopsies. In a case-control retrospective study in patients with traumatic brain injuries, infections with gram-negative *Pseudomonas* species were significantly associated with NHO development. Together these data suggest a functional association between gram-negative bacterial infections and NHO development and highlights infection management as a key consideration to avoid NHO development in patients. © 2023 The Authors. *Journal of Bone and Mineral Research* published by Wiley Periodicals LLC on behalf of American Society for Bone and Mineral Research (ASBMR).

KEY WORDS: OSTEOIMMUNOLOGY; CYTOKINES; DISEASES AND DISORDERS OF/RELATED TO BONE (OTHER); ANIMAL MODELS

Introduction

Neurogenic heterotopic ossifications (NHO) are pathological extraskeletal bones that develop in periarticular muscles

subsequent to severe injuries of the central nervous system (CNS), such as spinal cord injuries (SCI), traumatic brain injuries (TBI), cerebral strokes, or cerebral anoxia.⁽¹⁾ NHO prevalence can be high, around 15% to 45% in victims of SCI and 10% to 37% for traumatic

This is an open access article under the terms of the [Creative Commons Attribution-NonCommercial-NoDerivs](https://creativecommons.org/licenses/by-nc-nd/4.0/) License, which permits use and distribution in any medium, provided the original work is properly cited, the use is non-commercial and no modifications or adaptations are made.

Received in original form March 7, 2023; revised form July 24, 2023; accepted August 15, 2023.

Address correspondence to: Kylie Alexander, PhD; Jean-Pierre Lévesque, PhD, and Marjorie Salga, MD, PhD, Mater Research Institute—The University of Queensland, Translational Research Institute, 37 Kent Street, Woolloongabba, Queensland, 4102, Australia. E-mail: kylie.alexander@mater.uq.edu.au, jp.levesque@mater.uq.edu.au, and marjorie.salga@aphp.fr

Additional Supporting Information may be found in the online version of this article.

Journal of Bone and Mineral Research, Vol. 00, No. 00, Month 2023, pp 1–18.

DOI: 10.1002/jbmr.4905

© 2023 The Authors. *Journal of Bone and Mineral Research* published by Wiley Periodicals LLC on behalf of American Society for Bone and Mineral Research (ASBMR).

brain injuries.⁽²⁻⁴⁾ Their periarticular location drives their pathogenicity as NHO can reduce the range of motion to completely ankylose the affected joints, impairing patients' ability to sit, dress, and perform common daily tasks, thus increasing morbidity and delaying rehabilitation.^(5,6) NHO treatment is limited to surgical resection,^(1,6-10) and recurrence is observed in 6% of patients.⁽¹¹⁾

The pathobiology of NHO is still poorly understood,⁽¹²⁾ but several risk factors have been identified. Severity of CNS injury, mechanical ventilation, tracheotomy, autonomic dysregulation, muscle overactivity, coexisting fracture, and orthopedic surgery have all been found to be significantly associated with increased NHO prevalence.^(4,13-15) Systemic infection is one of several risk factors associated with significantly higher NHO prevalence.^(3,4,14,16) Urinary tract infections and pneumonia are all significantly associated with higher incidence of NHO.^(3,4,14,16) However, the importance of infections occurring directly after the accident and its role in NHO formation have not been specifically investigated and thus may be underestimated.

To better understand NHO pathobiology, we previously developed a mouse model of SCI-induced NHO in genetically unmodified mice, where mice undergo a spinal cord transection between thoracic vertebrae T₁₁ to T₁₃ together with a muscle injury induced via an intramuscular injection of the snake venom myotoxin cardiotoxin.⁽¹⁷⁾ This model revealed that NHO develop only when these two injuries are concomitant.^(17,18) Mineralized foci can be detected in injured muscles from as early as 4 days post-surgery and develop over a period of 2 weeks into mature mineralized heterotopic bone nodules (formed via intramembranous ossification) with osterix+/osteocalcin+ osteoblast-like cells present by 21 days post-surgery.^(17,19) Using this model, we have shown that monocytes/macrophages infiltrating the injured muscle are critical in promoting NHO development,⁽¹⁷⁾ whereas granulocytes and lymphocytes are dispensable.^(20,21) Further studies revealed that SCI drives a prolonged inflammatory response in injured muscles⁽²²⁾ with elevated and persistent expression of the inflammatory cytokines oncostatin M (OSM) and interleukin-1 (IL-1), which both promote NHO development.⁽²²⁻²⁴⁾

Considering that IL-1 and OSM signaling are both key mediators of the inflammatory response to infections,⁽²⁵⁻²⁷⁾ we hypothesized that the increased prevalence of NHO in patients with infections may be due to exacerbated inflammatory signaling in response to these infections. Therefore, we evaluated the role of infection in driving SCI-induced NHO.

Materials and Methods

Animals

C57BL/6 mice were sourced from the Animal Resource Centre (Perth, Australia). *Tlr4*^{tm1Aki} (*Tlr4*^{-/-}),⁽²⁸⁾ *Myd88*^{tm1Aki} (*Myd88*^{-/-})⁽²⁹⁾ mice were donated by Dr Antje Blumenthal (The University of Queensland Frazer Institute). *Ticam1*^{tm1Aki} (*Ticam1*^{-/-}) mice⁽³⁰⁾ were donated by Prof Mark Smyth (QIMR Berghofer Medical Research Institute). All mice had been backcrossed more than 10 times on a C57BL/6 background and bred as homozygote pairs to generate mice for this project. Mice were housed at the Translational Research Institute, under specific pathogen-free conditions, fed a standard diet chow with *ad libitum* water access and simulated diurnal cycle. Mice were randomly assigned into cages with a maximum of 5 mice per cage, where appropriate cages contained mixed animal cohorts (eg, 2-3 C57BL/6 and 2-3 knockout mice) and were co-housed for 5 to 7 days before surgery. All animal experimental procedures were approved by the Health Sciences Animal

Ethics Committee of The University of Queensland (2017AE000050, 2021AE000537 and 2021AE001177) and followed the Australian Code of Practice for the Care and Use of Animals for Scientific Purposes.

SCI-induced NHO mouse model

NHO mouse model was carried out as previously described in ~7- to 8-week-old female mice.^(17,23,24) Mice were administered 100 mg/kg ketamine, 10 mg/kg xylazine, and 1% isoflurane, and subsequently received a laminectomy on the dorsal spine and the spinal cord was transected with a scalpel blade between T₁₁ to T₁₃ and an intramuscular injection (i.m.) of cardiotoxin (CDTX) purified from the venom of *Naja pallida* (Latoxan, Portes les Valence, France; Supplemental Table S1) at 0.32 mg/kg in the hamstring muscles. Post-surgery, all mice received a subcutaneous injection of ciprofloxacin (10 mg/kg), buprenorphine (0.075 mg/kg). As SCI causes paraplegia, mouse bladders were expressed manually by gentle massage of the bladder twice daily throughout the experiments. Mice were given Bactrim (800 mg/L, Roche, Mannheim, Germany) in drinking water after surgical procedures as prophylaxis for bladder infections. Although we have observed that NHO development is similar in both males and females, only females are used in this study as bladder expression is easier in females and the risk of bladder infection is therefore reduced compared with males.⁽³¹⁾

LPS administration

γ-irradiated LPS purified from *Escherichia coli* strain 0111:B4 (Sigma-Aldrich, St. Louis, MO, USA; catalog #L4391) was administered to SCI mice either at the time of surgery via an intramuscular injection (co-mixed with CDTX) at 0.02, 0.06, 0.1, 0.15, 0.208, and 1.25 mg/kg of body weight, or injected intraperitoneally post-surgery on days 2, 4, and 6 at 1.25 mg/kg of body weight. Control mice were administered the same volume of PBS as a control for intramuscular injections or saline for intraperitoneal injections.

Tissue collection for histology

At predetermined endpoints, mice were euthanized by CO₂ asphyxiation or anesthetized in an isoflurane chamber and blood collected by cardiac puncture. Hindlimbs were fixed in 4% paraformaldehyde (Sigma-Aldrich), decalcified, and processed as previously described.^(21,23,24) Blood samples were collected under strict sterile conditions in a tissue culture hood equipped with high-efficiency particulate air filter, in tubes containing ethylenediaminetetraacetic acid (EDTA) (4 mM final for 1 mL blood collected). Plasma was isolated by centrifugation at 1000g for 10 minutes at 4°C, plasma was transferred to another tube and again similarly centrifuged before collection. The small and large intestine were cleaned with PBS, fixed with 10% neutral buffered formalin for 24 hours before being embedded in paraffin.

Hindlimbs were fixed and decalcified and processed as previously described.⁽¹⁷⁾ Five-μm sections were cut and stained using Masson's Trichrome. In brief, sections were deparaffinized and rehydrated, then stained for 10 minutes in Weigert's iron hematoxylin, rinsed under tap water for 10 minutes, developed in 1% acid alcohol, 1% hydrochloric acid in water for 15 to 30 seconds, rinsed in tap water (3 minutes) then distilled water, followed by staining in Biebrich scarlet-acid fuchsine solution for 10 to 15 minutes (Biebrich scarlet, 1% aqueous, acid fuchsine, 1%

glacial acetic acid). Slides were then washed in distilled water and differentiated in 5% phosphomolybdic – 5% phosphotungstic acid solution for 10 to 15 minutes or until collagen is not red. Slides were transferred into aniline blue solution for 5 to 10 minutes and rinsed in 1% acetic acid for 2 to 5 minutes, dehydrated, and mounted in resinous mounting medium. Immunohistochemistry (IHC) was performed as previously described.^(21,23,24) Primary antibodies: rat anti-mouse F4/80 monoclonal antibody (mAb) (Novus Biologicals, Littleton, CO, USA), rabbit anti-mouse Osterix/Sp7 mAb (Abcam, Cambridge, UK), rabbit anti-mouse osteocalcin (polyclonal Ab) (Enzo Life Sciences, Farmingdale, NY, USA) or relevant isotype control antibodies; rabbit IgG (Abcam) or rat IgG2b (BioLegend, San Diego, CA, USA). A 3-step procedure using biotinylated F(ab)2 secondary antibodies (biotinylated goat anti-rat IgG and goat anti-rabbit IgG) (Vector Labs, Burlingame, CA, USA) and VECTASTAIN Elite ABC-Peroxidase Kit (Supplemental Table S1) was used to detect primary antibodies. All slides were viewed using an BX50 microscope (Olympus, Tokyo, Japan) with an attached DP26 camera and imaged using Olympus CellSens standard 1.7 imaging software (Olympus).

Purification of muscle progenitors and leukocytes for RNA extraction

Total muscle leukocytes were isolated from C57BL/6 mouse hamstring muscles 4 days post CDTX muscle injury using a skeletal muscle dissociation kit (Miltenyi Biotech, Bergisch Gladbach, Germany) as per manufacturer's instructions. Total muscle leukocytes were sorted into multiple populations using a BD FACS Aria Fusion (BD Biosciences, Franklin Lakes, NJ, USA) using fluorescent monoclonal antibodies (BioLegend) CD45-BV785 (clone 30-F11), anti-TER119-FITC (clone TER119), CD45R/B220-FITC (clone RA3-6B2), CD3 ϵ -FITC (clone 145-2C11), CD11b-PE (clone M 1/70), anti-F4/80-APC (clone BM8), anti-anti-Ly6C-Pacific Blue (Clone HK1.4) and anti-Ly6G-PECY7 (clone 1A8), and cell viability with FVS700. Monocytes/macrophages were sorted as CD45⁺ Ter119⁻ B220⁻ CD3 ϵ ⁻ CD11b⁺ F4/80⁺ CD48⁺ Ly6G⁻ with various levels of Ly6C expression, granulocytes as CD45⁺ Ter119⁻ B220⁻ CD3 ϵ ⁻ CD11b⁺ F4/80⁻ CD48⁻ Ly6G⁺. Muscle progenitor cells were isolated from hamstring muscles of naïve C57BL/6 muscles and stained with the following fluorescent monoclonal antibodies: CD45-BV785 (clone 30-F11), anti-TER119-FITC (clone TER119), CD45R/B220-FITC (clone RA3-6B2), CD3 ϵ -FITC (clone 145-2C11), CD11b-FITC (clone M 1/70), anti-Gr1-FITC (clone RB6-8C5), CD31-BV421 (clone 390), anti-Sca1-PECY7 (clone D7), CD34-e660 (clone RAM34), anti-PDGFR α -PE (clone APA5) and anti-integrin α 7-PE (clone R2F2) and cell viability with FVS700. Populations were sorted using a BD FACS Aria Fusion according to the following phenotypes: satellite cells (SC): CD45⁻ lineage-(Ter119, B220, CD3 ϵ , CD11b, Gr1)⁻ CD31⁻ CD34⁺ Sca1⁻ integrin α 7⁺ PDGFR α ⁻; fibroadipogenic progenitors (FAP) CD45⁻ Lin⁻ CD31⁻ CD34⁺ Sca1⁺ integrin α 7⁻ PDGFR α ⁺ as previously described.⁽¹⁹⁾ All populations were sorted directly into 1 mL Trizol LS (Thermo Fisher Scientific, Waltham, MA, USA) and frozen until extraction.

RNA extraction and qRT-PCR

For RNA isolation of muscle, frozen muscle samples were homogenized in Trizol (Life Technologies, Carlsbad, CA, USA) using a TissueRuptor (Qiagen, Valencia, CA, USA), and after chloroform separation, RNA was isolated from aqueous phase. mRNA was isolated from sorted cells using chloroform separation from

initial Trizol preparation followed by GeneJET RNA cleanup and concentration micro kit (Thermo Fisher Scientific). Reverse transcription was performed with all RNA samples using the SensiFAST cDNA Synthesis Kit (Thermo Fisher Scientific) as per manufacturer's instructions. mRNA expression was analyzed using a single-step reverse transcription quantitative real-time polymerase chain reaction (qRT-PCR) on ViiA 7 Real-Time PCR System (Life Technologies) with PCR setting: 20 seconds at 95°C, then 40 cycles of 95°C (1 second) and 60°C (20 seconds). Taqman system using TaqMan fast PCR Master Mix and TaqMan (Supplemental Table S1). Ct values were normalized by the expression of the housekeeping genes *Rps20* (for whole muscle) or *Hprt* (for sorted cells) and presented as ratio to house-keeping gene (delta CT method).

Flow cytometry analysis of muscle progenitors and macrophages

Total leukocytes from naïve C57BL/6 muscle were isolated as described above and multiple populations identified using a CytoFLEX benchtop flow cytometer equipped with 405, 488, 561, and 637 nm solid phase lasers (Beckman Coulter Life Sciences, Brea, CA, USA) using the following fluorescent mAb (BioLegend): FITC anti-mouse Ter119, PE/Cyanine7 anti-mouse Ly-6A/E (Sca-1), PE anti-mouse CD284 (TLR4), APC/Cy7 anti-mouse CD45, Brilliant Violet 421 anti-mouse CD31, and Zombie Aqua Fixable Viability Kit, as well as eFluor 660 anti-mouse/human CD34 (Thermo Fisher Scientific) (antibodies listed in Supplemental Table S2). At 4 days post-surgery, total leukocytes from muscle were isolated using a skeletal muscle dissociation kit (Miltenyi Biotech). Total leukocytes were subsequently discriminated into multiple populations using a CytoFLEX benchtop flow cytometer using the following mAb (BioLegend; outlined in Supplemental Table S1): FITC anti-mouse Ter119, FITC anti-mouse B220, FITC anti-mouse CD3 ϵ , APC anti-mouse F4/80 (clone BM8), PE/Cy7 anti-mouse Ly6G, Brilliant Violet 510 anti-mouse/human CD11b, Brilliant Violet 785 anti-mouse CD45, and BD Horizon Fixable Viability Stain 700 (Supplemental Table S1). Files were subsequently analyzed with Flow Jo software version 10.5 (Becton Dickinson & Company, San Diego, CA, USA).

Blood collection for quantification of plasma cytokines

For plasma isolation, blood samples were taken from mice by terminal cardiac puncture 17 or 72 hours post-injury under anesthesia (2% to 3% isoflurane). Blood was collected in tubes containing EDTA (4 mM final for 1 mL blood collected) and plasma was isolated by centrifugation (1000g for 10 minutes). Plasma was subsequently transferred into new tubes and spun again (1000g for 10 minutes) and plasma stored at -80°C until use. Plasma cytokine concentrations were measured in triplicate using bead-based immunoassay (LEGENDplex, mouse inflammation panel, BioLegend, catalog #740150) and analyzed on a CytoFLEX benchtop flow cytometer.

Plasma OSM concentrations were measured using a mouse Oncostatin M DuoSet ELISA Kit (DY495-05, R&D Systems, Minneapolis, MN, USA) and Ancillary Reagent Kit as per manufacturer's instructions in duplicates including standards. Plates were read with plate reader (Thermo Fisher Scientific) according to manufacturer's instructions.

Micro-computed tomography (μ CT) and NHO volume quantification

Because of instrument upgrades during the course of this study, NHO volumes were measured either *in vivo* or *ex vivo* using either the Inveon positron emission tomography/computed tomography (PET-CT) multimodality system (Siemens Medical Solutions Inc., Malvern, PA, USA) or the Molecubes β -Cube and X-Cube μ PET-CT system (Molecubes, Gent, Belgium). For samples measured using the Inveon, parameters were: 360° rotation, 180 projections, 500 ms exposure time, 80 kV voltage, 500 μ A current, and an effective pixel size of 36 μ m. 3D reconstitutions were performed using the Inveon Research Workplace software (Siemens Medical Solutions Inc.). For samples measured with Molecubes β -Cube, 3D reconstitutions and NHO volumes were quantified using VivoQuant 2021 (In vivo, Needham, MA, USA). To quantify NHO volumes, the region of interest (ROI) was drawn around the muscles containing NHO, and these were then carefully checked from three dimensions to ensure adjacent long bones were not included in the ROI. Calcified NHO regions were defined as above the threshold of 450 Hounsfield units (HU).^(21,23,24)

Gut permeability quantification and histopathological scoring

Mice underwent either SCI or SHAM (incision of the dorsal skin only) surgery with an intramuscular injection of CDTX. From the evening of day 6 post-surgery, mice were fasted overnight. The next morning, all mice were administered 600 mg/kg 4 kDa FITC-dextran (Sigma-Aldrich, catalog #46944) dissolved in sterile PBS via oral gavage. Blood was collected by terminal cardiac puncture under general anesthesia 4 hours later and plasma was collected as described above. As a positive control (known intestinal permeability), plasma was also collected from mice with acute colitis induced by dextran sodium sulphate (DSS). These mice received 3% (w/v) 40 kDa DSS (Sigma-Aldrich, catalog #42867) in their drinking water for 7 consecutive days as previously described.^(32,33) Fifty microliters of plasma was added to individual wells of a black 96-well plate, along with serial dilutions of a FITC-dextran calibration standard. Fluorescence was measured on a PHERAStar FS plate fluorimeter (BMG Labtech, Ortenberg, Germany) with an excitation at 485 nm and emission at 520 nm.

For histopathology scoring on small and large intestine, sections were dewaxed and stained with hematoxylin–eosin. Sections were visualized at 8 \times magnification lens using an Olympus BX50 microscope with an attached DP26 camera and imaged using Olympus CellSens standard 1.7 imaging software. The duodenum and colon were chosen to study the extent of inflammation in small and large intestines, respectively. Both the epithelium and mucosa were examined and scored based on (i) inflammatory cell infiltration (scores from 1 to 4), (ii) changes in the epithelial layer (scores 0 to 5), and (iii) changes in mucosal architecture (scores 0 to 5), and the 3 scores added together to give a total score as previously described⁽³⁴⁾ with a score from 0 for healthy gut to a maximum of 14.

Measurements of blood bacterial load and endotoxemia

Bacterial load in plasma was measured by quantitative real-time PCR for the 16s rRNA genes. Total DNA from mouse blood was extracted using the Maxwell 16 Blood DNA Purification Kit (Promega, Madison, WI, USA; catalog #AS1010). Samples were processed as per the manufacturer's instructions and run on

the Maxwell 16 Instrument (Promega, catalog #AS3000). To verify the DNA isolation procedure, blood from SCI mice was spiked with mouse feces before DNA purification. DNA extracted from blood samples were subjected to real-time PCR analysis in QuantStudio 7 Flex Real-Time PCR System (Thermo Fisher Scientific, catalog #4485701) using universal 16s rRNA forward primer (5'-GAATTGRCGGGRC-3'; 917F; Integrated DNA Technologies, Coralville, IA, USA) and reverse primer (sequence – 5'-ACGGGCGGTGWGTRC-3'; 1392R; Integrated DNA Technologies) with SYBR green qPCR master mix (Thermo Fisher Scientific, catalog #K0241) to detect the presence of 16s rRNA gene. As positive controls for the amplification, whole bacterial DNA were run in duplicates at 0.6 ng, 6 ng, and 60 ng. Plasma samples of mice from naïve, SHAM-operated and SCI groups with CDTX-injured muscles were tested for endotoxin using an Endotoxin ELISA Kit (Aviva Systems Biology, San Diego, CA, USA; catalog #OKEH02559). Blood plasma samples from mice with acute colitis induced by 7 days of drinking water containing 3% 40 kDa DSS were used as positive controls for endotoxemia.

Human study approvals

Muscle samples were obtained with the informed consent of the patients and the approval from the Comité de Protection des Personnes (CPP approval n°09025) and from the National Commission Nationale de l'Informatique et des Libertés (CNIL approval no. Eyo1066211J).

As this retrospective study was noninterventional with best practice procedures and without additional interventions, patients' consent was not needed. The authors confirm that the named institutional review board specifically waived the need for consent for this study (Comité de Protection des Personnes, Ile de France XI, Pavillon Jacques Courtois – 2ème étage 20, rue Armagis 78105 Saint Germain en Laye Cedex. Tel: 0139274258. Fax: 0139274901. E-mail: ccppidf11@chi-poissy-st-germain.fr). According to the French law from January 6, 1978, amended in 2004, the present work has been declared to the French Commission Nationale de l'Informatique et des Libertés (CNIL) no. 2212374 v 0).

Isolation of human PDGFR α ⁺ cells from NHO biopsies

Muscle surrounding NHOs were collected from NHO surgical waste after their excision from 4 patients with brain injury, spinal cord injury, or stroke. NHO resection surgeries were performed at Raymond Poincaré Hospital (Garches, France). Muscle fragments were minced using scalpel and small scissors, placed in a 50 mL Falcon tube, and incubated in 1.5 mg/mL pronase (Sigma-Aldrich, catalog #10165921001) in α -MEM, 45 minutes in a 37°C water bath. After addition of α -MEM supplemented with 15% FCS and 1% antibiotics, the cell suspension was filtered through a 100 μ m cell strainer, then a 40 μ m cell strainer (BD Falcon). Isolated muscle progenitor cells (MuPCs) were maintained in α -MEM supplemented with 15% FCS, 1% antibiotics and 10 ng/mL basic fibroblast growth factor (bFGF) (R&D Systems). Human MuPCs were trypsinized and incubated 30 minutes with biotinylated anti-human PDGFR α (clone 16A1, R&D Systems) and CD56-PE (clone B159, BD Pharmingen) monoclonal antibodies in PBS 2% FCS, 2 mM EDTA. Cells were washed and incubated 30 minutes with Streptavidin-APC/Cy7 and the viability dye 7-actinomycin D (Sony). Cells were washed and filtered through a 30 μ m cell strainer (Sysmex, Kobe, Japan) and sorted using a FACSAria III SORP sorter (BD Biosciences). PDGFR α ⁺ CD56⁻ cells (FAPs)⁽¹⁹⁾ were seeded at 3000 per cm² in α -MEM supplemented with 20% FCS, 1% antibiotics, and 10 ng/mL bFGF (R&D Systems).

In vitro osteogenic differentiation and quantification of mineralization of human PDGFR α ⁺ cells

PDGFR α ⁺CD56⁻ cells were seeded in 24-well plates at 3000 per cm² in α MEM supplemented with 10% FCS and 1% antibiotics. Once cells adhered to the wells, medium was replaced by α MEM supplemented with 10% FCS, 1% antibiotics, and 0.052 μ g/mL dexamethasone, 12.8 μ g/mL ascorbic acid, and 2.15 mg/mL β -glycerophosphate (Sigma-Aldrich) to induce osteogenic differentiation. LPS was added at 1, 10, or 100 ng/mL. Cells were cultured for 14 days at 37°C in 5% CO₂ atmosphere, and medium was changed twice a week. Quantification of mineralization was performed using Alizarin Red S staining. Cells were washed with PBS, fixed in 70% ethanol, quickly washed with distilled water, and incubated 5 minutes in 20 g/L Alizarin Red S, pH = 4.2 (Sigma-Aldrich). Cells were washed with distilled water and dried. Alizarin Red S dye was extracted with 0.5 N hydrochloric acid and 5% SDS and quantified by spectrophotometry at 405 nm.

qRT-PCR of human muscle PDGFR α ⁺ cells

After 7 days of osteogenic differentiation, PDGFR α ⁺ CD56⁻ cells were lysed in Qiazol (Qiagen) followed by chloroform/isopropanol total RNA extraction. Reverse transcription was performed using QuantiTect Reverse Transcription Kit (Qiagen). qRT-PCR were performed on a LightCycler 480 instrument (Roche) using QuantiTect SYBR Green RT-PCR Kit and QuantiTect Primers (Qiagen) (Supplemental Table S1). Three housekeeping gene mRNAs (*RPLPO*, *PPIA*, *HPRT*) were selected based on their expression stability using geNorm analysis. *ALPL* and *RUNX2* mRNA quantification were performed as the geometric mean of the quantifications obtained with each reference RNA.

Retrospective control–case study in TBI patients

A case–control design was used for this study, following guidelines for epidemiological studies⁽³⁵⁾ because of the low numbers of TBI-related NHO in this patient group. Case and control patients were all treated in the same intensive care unit (ICU) department and the same head injury rehabilitation center.

Participants: Patients enrolled in this study were all admitted for TBI in the same ICU of a tertiary care Hospital (Hôpital Beaujon, Assistance Publique des Hôpitaux de Paris, France) for vital care and the same neurorehabilitation center (Hôpital Raymond Poincaré, Assistance Publique des Hôpitaux de Paris, France) between January 2016 to June 2018. In this population of patients, we then stratified TBI patients with and without NHO. Patients involved in the study had surgical excision for troublesome NHO by the same surgeon in the orthopedic department. Patients were excluded if they developed a NHO before the TBI.

Outcome measures: Medical records that contained complete details of the patient's medical history were compared in order to (i) confirm and document the relationship between infection and NHO at an early stage after TBI in a context of polytrauma and (ii) define precocious inflammatory factors (circumstances of the accident, neurological and respiratory state, drugs used, associated trauma) involved in NHO development.

Data collection: The data were obtained via the Medical Database of ICU department and “Head Injury Database” database. We listed for each patient the age at the time of the accident (years), the sex, and the body mass index (BMI) (kg/m²). The following data related to infections in ICU were recorded for each patient: infection location (pulmonary, urinary, cutaneous,

abdominal), number of sepsis-related infection⁽³⁶⁾ and septic shock⁽³⁷⁾ during ICU stay, bacteria family (gram-negative, gram-positive, non-documented) and individual bacteria species for each infection, polymicrobial infections, and delay from TBI to the first infection (days).

Inflammatory factors were also recorded: duration of stay in ICU (days), duration of coma (days), circumstances of the accident (TBI etiology, velocity, crush-projection of the body during the accident, presence of alcohol in the first blood test), neurological and respiratory state, drugs used, associated trauma.

Neurological state after TBI was investigated using: the first Glasgow Coma score recorded, intracranial lesions on the first CT scan, increase in intracranial pressure >25 mmHg, associated traumatic spinal cord injury, and motor and cognitive disorder (time and space orientation) at patient's discharge from ICU.

Respiratory state was defined by the duration of oro-tracheal intubation (days), duration of mechanical ventilation (days), implantation of tracheotomy, and acute respiratory distress syndrome. Information about patient drug treatments was recorded, including the types of drugs used, the duration of the prescription (days), and the dose administered.

Associated traumas were also recorded, including the number of bone fractures, number of surgeries for bone fracture, number of chest-pelvis-abdominal traumas sustained and surgery or drain implantation for chest-pelvis-abdominal trauma, craniectomy, craniotomy, extracranial cerebrospinal fluid derivation, and injury severity score (ISS).⁽³⁸⁾

The Sequential Organ Failure Assessment (SOFA) score was calculated 24 hours after the accident to evaluate the degree of organ dysfunction in the patients studied.^(39,40) The Simplified Acute Physiological Score II (SAPS II) estimates mortality in ICU patients and was collected within the first 24 hours of ICU admission.⁽⁴¹⁾ Other complications previously related to NHO were also collected, such as bedsores and deep venous thrombosis.

Statistical analyses

For mouse experiments, data are presented in boxplots with median with maximum and minimum values. Statistically significant differences were determined using either two-sided Mann–Whitney test, one- or two-way ANOVA, or nonparametric Friedman test using Prism software (version 8.0; GraphPad Software, La Jolla, CA, USA).

For the correlative study in TBI patients, data are described as their frequencies and percentages for the categorical variables and as their medians (25th–75th percentile range) for the quantitative variables. Univariate analysis was then performed. Categorical variables were compared using the chi-square test or the Fisher exact test as appropriate and quantitative variables using Wilcoxon's ranked-sum test. All tests were two-sided, and statistical significance was set at the $p = 0.05$ level.

Results

LPS purified from gram-negative bacteria exacerbates NHO development after SCI in mice

Most pathogens causing nosocomial infections in ICU are gram-negative bacteria such as *Enterobacteriaceae*, *Acinobacter* species, *Bacteroides fragilis*, and *Pseudomonas aeruginosa*.⁽⁴⁰⁾ As LPS production is exclusive to the wall of gram-negative bacteria, we used purified LPS in our mouse model of SCI-NHO to mimic a local infection by gram-negative bacteria.

We first performed a titration to investigate the effect of local LPS administration to NHO development. Mice received a SCI and a muscle injury via an intramuscular CDTX injection, where increasing doses of LPS were mixed with the CDTX before injection. NHO bone volumes were measured at 7 days post-surgery

via μ CT. This dose range of LPS was selected based on previous experiments in our laboratory and other published models using intramuscular LPS injections.⁽⁴²⁾ Doses started at 0.025 mg/kg up to 1.25 mg/kg, all doses well below lethal dose.⁽⁴³⁾ Compared with LPS administration at 0.025 mg/kg, LPS at 0.15 mg/kg and

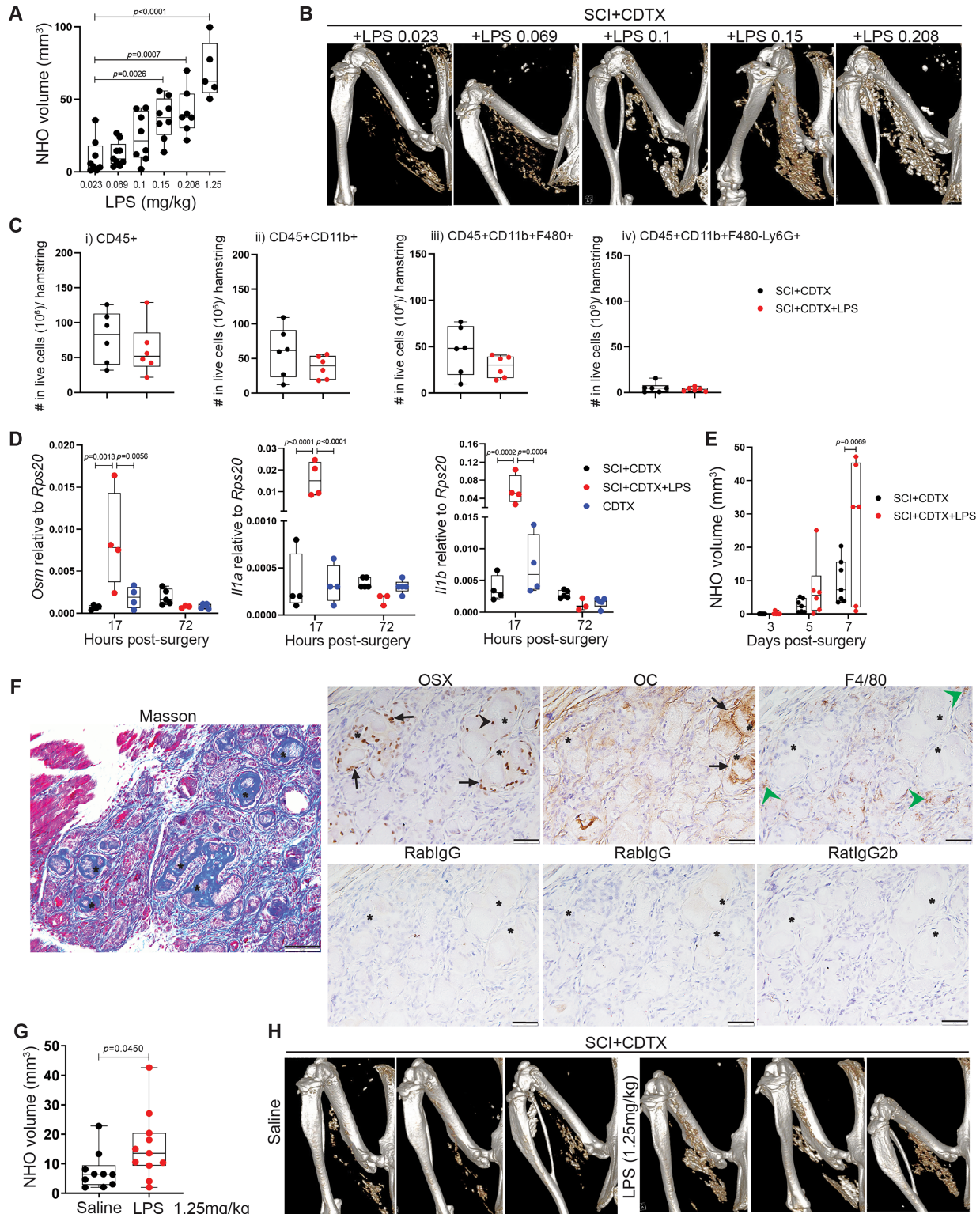


(Figure legend continues on next page.)

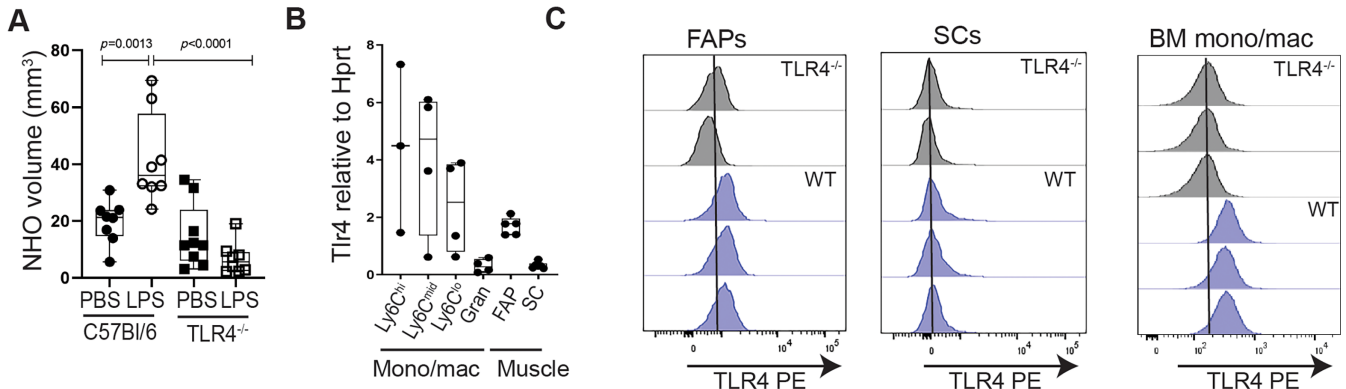


Fig. 2. Lipopolysaccharide (LPS) exacerbates spinal cord injury (SCI)-induced neurogenic heterotopic ossifications (NHO) via TLR4. (A) NHO volumes quantified at 7 days post-surgery in C57BL/6 or *Tlr4*^{-/-} mice that underwent SCI + CDTX co-injected intramuscularly with either PBS or LPS (0.15 mg/kg). (B) Expression of *Tlr4* mRNA transcript in sorted muscle monocytes/macrophages (CD45⁺ Ter119⁻ B220⁻ CD3e⁻ CD11b⁺ F480⁺ Ly6C^{hi/mid/lo}), granulocytes (gran) (CD45⁺ CD11b⁺ F4/80⁻ Ly6G⁺), or muscle fibroadipogenic progenitors (FAPs) (CD45⁻ Lin⁻ CD31⁻ Sca1⁺ CD34⁺) and satellite cells (SCs) (CD45⁻ Lin⁻ CD31⁻ Sca1⁻ CD34⁺) 4 days post SCI + CDTX. All dots represent an individual mouse, data in (A) two independent experiments, presented as median with interquartile ranges, using a one-way ANOVA with Sidak multiple comparison test. (C) TLR4 surface expression in muscle FAPs and SCs, as well as BM monocyte/macrophage cells (positive control for TLR4 surface expression), in both wild-type (WT) and *Tlr4*^{-/-} mice. Each profile represents a different mouse; black vertical bar is placed on the peak of the histograms for cells from *Tlr4*^{-/-} mice as negative controls.

above showed a significant increase in NHO volumes at 7 days post-surgery (Fig. 1A, B).

We have previously shown in injured muscles developing NHO that expression of the pro-inflammatory cytokines OSM, IL-1 β , and IL-1 α is abnormally elevated compared with injured muscles without SCI at 2 or 4 days post-injury.^(22,23) To investigate whether increased NHO bone volumes after LPS administration was due to enhanced innate immune responses, we quantified the absolute numbers of multiple innate immune populations in hamstring muscles 4 days post-surgery, a time

point that we have previously confirmed as the peak of macrophage infiltration. Mice received a SCI and a muscle injury via CDTX injection, co-injected with either saline or 0.15 mg/kg of LPS (the minimum LPS concentration that displayed significantly increased NHO bone volumes in Figure 1A). There were no significant changes to total CD45⁺ leukocytes, CD45⁺CD11b⁺ myeloid cells, CD45⁺CD11b⁺Ly6G⁻F4/80⁺ monocytes/macrophages, or CD45⁺CD11b⁺Ly6G⁺F4/80⁻ granulocytes after LPS treatment (Fig. 1C). In sharp contrast, mRNA encoding OSM, IL-1 α and IL-1 β were significantly upregulated 12-fold, 49-fold, and 16-fold,

(Figure legend continued from previous page.)

Fig. 1. Lipopolysaccharide (LPS) exacerbates spinal cord injury (SCI)-induced neurogenic heterotopic ossifications (NHO) in a dose-dependent manner in mice. (A, B) NHO volumes quantified at 7 days post-surgery by μ CT in C57BL/6 mice, which underwent SCI surgery and muscle injury induced via an i.m. injection of CDTX, co-injected with increasing doses of LPS with representative μ CT images at 7 days post-surgery. Each dot represents an individual mouse. Data are from two independent experiments and presented as median with interquartile ranges, using a one-way ANOVA with Dunnett's multiple comparison test. (C) C57BL/6 mice underwent SCI surgery and intramuscular injection of CDTX alone or in combination with 0.15 mg/kg LPS. Muscle leukocytes were extracted from hamstrings at 4 days post-surgery and frequencies of each leukocyte population relative to total live muscle cells per hamstring were quantified by flow cytometry. Populations were identified as (i) total CD45⁺ leukocytes (FVS700⁻, CD45⁺), (ii) Total CD11b⁺ myeloid cells (FVS700⁻, CD45⁺, CD11b⁺), (iii) monocytes/macrophages (FVS700⁻, CD45⁺, CD11b⁺, Ly6G⁻, F4/80⁺), and (iv) granulocytes (FVS700⁻, CD45⁺, CD11b⁺, F4/80⁻, Ly6G⁺). Each dot represents an individual mouse. Data from a single experiment, presented as median with interquartile ranges. (D) C57BL/6 mice underwent CDTX muscle injury alone, or SCI + CDTX or SCI + CDTX in combination with 0.15 mg/kg LPS. Relative mRNA expression for inflammatory cytokines *Osm*, *Il1a*, or *Il1b* in hamstrings 17 and 72 hours post-injury. Each dot represents an individual mouse. Data from a single experiment, presented as median with interquartile ranges, using a two-way ANOVA with Tukey's multiple comparisons test. (E) C57BL/6 mice underwent SCI + CDTX or SCI + CDTX in combination with 0.15 mg/kg and NHO volume was quantified at 3, 5, and 7 days post-surgery. Each dot represents an individual mouse, data from a single experiment, presented as median with interquartile ranges, using a two-way ANOVA with Sidak's multiple comparisons test. (F) Masson's Trichrome and immunohistochemistry for osterix (OSX), osteocalcin (OC), and F4/80 expression in serial sections of hamstring muscles from C57BL/6 21 days post SCI + CDTX + LPS (1.25 mg/kg i.m.). Numerous NHO foci are present within the injured muscle (*). Osterix⁺ cells are noted on NHO foci (arrows) and can also be embedded within the NHO matrix (arrowhead). NHO foci also express osteocalcin on bone surfaces (arrows) and are surrounded by F4/80⁺ macrophages (green arrowheads). * symbols also denote the same anatomical landmarks in each serial section. (G, H) NHO volumes at 7 days post-surgery in C57BL/6 mice, which underwent SCI surgery and CDTX muscle injury and subsequently administered saline or LPS (1.25 mg/kg of body weight) via intraperitoneal injection at days 2, 4, and 6 post-surgery, with representative μ CT images at 7 days post-surgery. Each dot represents an individual mouse. Data are from two independent experiments and presented as median with interquartile ranges and Mann-Whitney test.

respectively, in injured muscles of SCI + CDTX mice that received LPS compared with mice with SCI + CDTX without LPS, as early as 17 hours post-injury (Fig. 1D). At 72 hours post-injury, treatment with LPS had no more significant effect on expression of these cytokines in injured muscles compared with SCI + CDTX mice without LPS. Consistent with our previous findings,^(22,23) expression of OSM and IL-1 β mRNA at 72 hours was higher in injured muscles of mice with SCI + CDTX injury compared with CDTX injury alone, but this was not significant in a two-way ANOVA. This early pro-inflammatory cytokine spike remained confined within the injured hamstring muscle as no changes were detected for these cytokines in the plasma at either time point (Supplemental Fig. S1).

To determine whether this early pro-inflammatory cytokine spike in injured muscles of mice treated with LPS may cause an acceleration of NHO development, we performed a longitudinal analysis by live μ CT imaging at earlier time points (3, 5, and 7 days post-injury) (Fig. 1E). Intramuscular LPS injection at the site of injury did not accelerate NHO formation but amplified it from day 5 onward.

Masson's trichrome staining at 21 days post-surgery in SCI + CDTX + LPS mice showed abundant collagen I deposition with numerous NHO foci present throughout injured muscle (Fig. 1F). Similar to mice that develop NHO in the absence of LPS,^(17,22,23) NHO foci were associated with osterix+ and osteocalcin+ osteoblast lineage cells and F4/80+ macrophages (Fig. 1F). Next, to mimic a systemic infection (endotoxemia), we injected LPS intraperitoneally at 2, 4, and 6 days after surgery (Fig. 1G, H) at 1.25 mg/kg (the highest LPS dose tested via intramuscular injection in Fig. 1A). Similar to local administration of LPS, systemic administration also significantly increased NHO volumes compared with saline injected mice.

LPS increased NHO size via TLR4 receptors and TRIF

The LPS receptor is composed of transmembrane protein TLR4 dimers complexed with its obligatory partner protein myeloid differentiation factor-2 (MD-2).^(44,45) To demonstrate the effect of LPS was specifically mediated by TLR4, C57BL/6 and *Tlr4*^{-/-} mice underwent SCI and intramuscular CDTX injection together with PBS or LPS at 0.15 mg/kg (the minimum LPS concentration

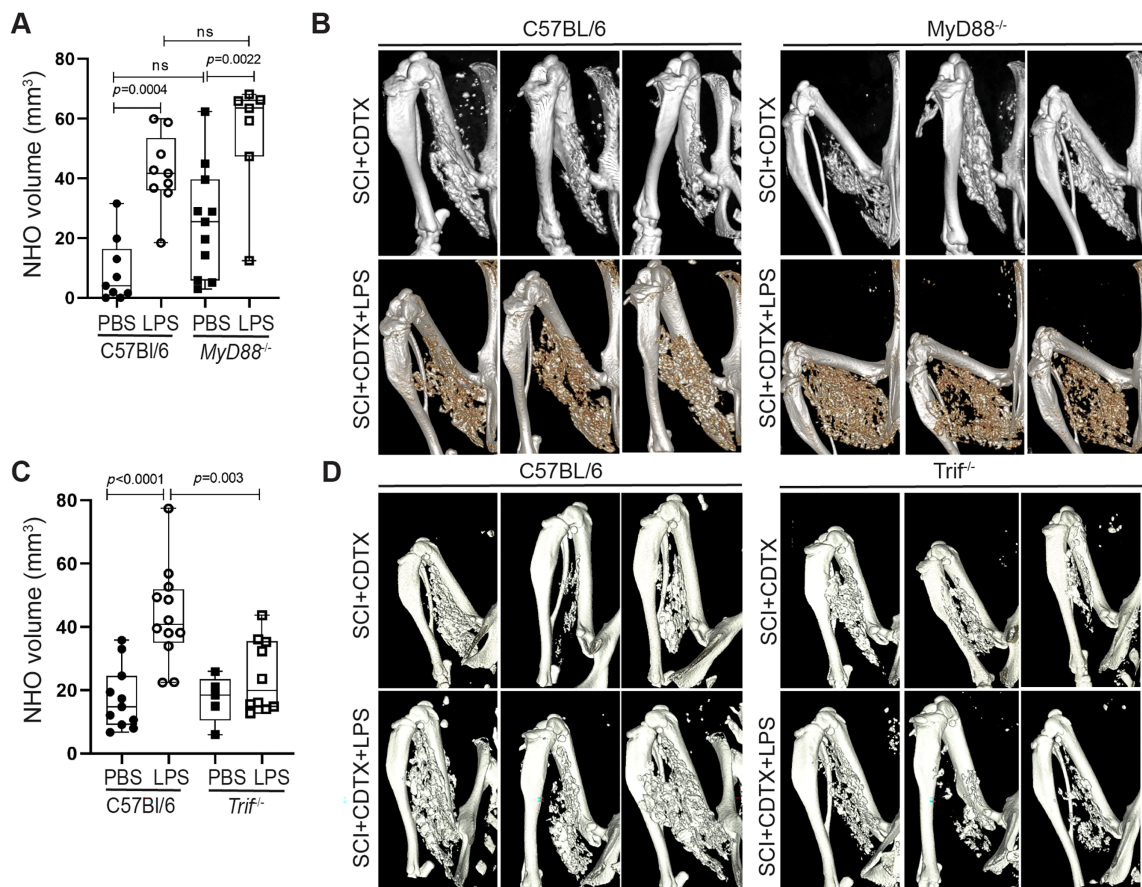


Fig. 3. Lipopolysaccharide (LPS) exacerbates spinal cord injury (SCI)-neurogenic heterotopic ossifications (NHO) via the endosomal TLR4/TRIF pathway. (A, B) NHO volumes quantified at 7 days post-surgery in C57BL/6 and *Myd88*^{-/-} mice that underwent SCI + CDTX, co-injected intramuscularly with either PBS or LPS (0.15 mg/kg), with representative μ CT images at 7 days post-surgery. (C, D) NHO volumes quantified at 7 days post-surgery in C57BL/6 or *Ticam1*^{-/-} mice that underwent SCI + CDTX, co-injected intramuscularly with either PBS or LPS (0.15 mg/kg), with representative μ CT images at 7 days post-surgery. All dots represent an individual mouse, two independent experiments, presented as median with interquartile ranges, using a one-way ANOVA with Sidak multiple comparison test.

that displayed significantly increased NHO bone volumes in Fig. 1A). NHO volumes measured at 7 days post-surgery demonstrated that while LPS significantly increased NHO in C57BL/6 mice, LPS had no effect in *Tlr4*^{-/-} mice (Fig. 2A), thereby establishing that the enhancing effect of LPS on NHO formation is mediated by TLR4.

The expression *Tlr4* mRNA has been shown in both immune and non-immune cell populations, including mesenchymal cells.⁽⁴⁶⁾ Therefore, we investigated which cell populations present in muscle have the potential to respond to LPS via expression of TLR4. We sorted multiple immune and non-immune cell populations from mouse hamstring muscles, including Ly6C^{bright}, Ly6C^{low}, and Ly6C⁻ monocytes/macrophages,

granulocytes, and mesenchymal fibro-adipogenic progenitors (FAPs), which are the cells-of-origin of NHO,⁽¹⁹⁾ and satellite cells (SCs), which are the myogenic stem cells,⁽⁴⁷⁾ to quantify *Tlr4* mRNA expression by qRT-PCR. All Ly6C monocyte/macrophage subsets and muscle FAPs expressed *Tlr4* transcripts, whereas granulocytes and SCs expressed *Tlr4* transcripts at approximately 10-fold lower levels (Fig. 2B).

To confirm these data at the protein level, we isolated muscle FAPs and SCs from C57BL/6 or *Tlr4*^{-/-} mice that were stained for TLR4 cell surface expression analyzed by flow cytometry. Bone marrow myeloid cells from the same mice were used as positive controls. TLR4 cell surface staining (Fig. 2C) confirmed the transcriptional data, illustrating that muscle FAPs transcribe and

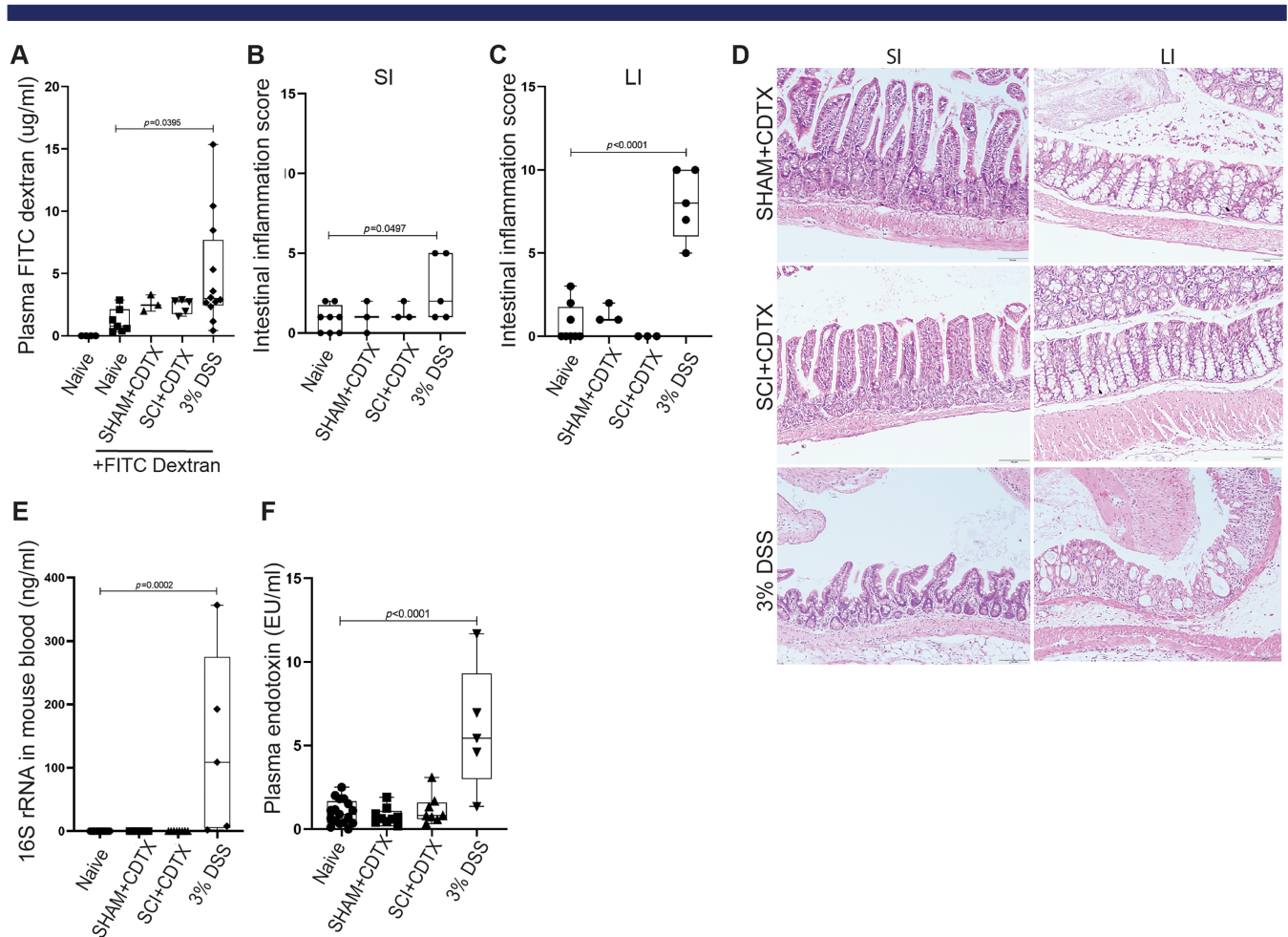


Fig. 4. Spinal cord injury (SCI) at vertebrae T₁₁ to T₁₃ does not cause gut leakage in the SCI-neurogenic heterotopic ossifications (NHO) mouse model. (A) FITC-dextran concentration in blood plasma 7 days post-SCI or sham surgeries with an intramuscular injection of CDTX (0.32 mg/kg). Mice with 3% DSS-induced colitis (3% DSS) were performed as positive controls. FITC-dextran (4 kDa) was administered by oral gavage 12 hours post-fasting, and blood collected 4 hours later to measure FITC-dextran leakage into blood plasma. (B, C) Histopathology scores for intestinal inflammation in either small (SI) or large intestine (LI), in naïve or sham + CDTX and SCI + CDTX and mice 7 days post-surgery, or 3% DSS-treated mice as positive controls. (D) Representative images of hematoxylin and eosin (H&E) staining from both SI and LI in sham + CDTX or SCI + CDTX mice 7 days post-surgery, illustrating negligible inflammatory infiltrate, with no hyperplasia, ulceration, goblet cell loss, or abnormal crypts across the epithelium and mucosa, 3% DSS-treated mice included as positive controls. Images 20× magnification; scale bar = 100 μm. (E) Quantification of prokaryote 16S rRNA gene in blood of naïve, and sham + CDTX or SCI + CDTX mice 7 days post-surgery. Three-percent DSS-induced colitis mice were used as positive controls. (F) Plasma endotoxin concentration was measured by ELISA from either naïve, sham + CDTX, or SCI + CDTX mice 7 days post-surgery. Three-percent DSS-induced colitis mice were used as positive controls. Each dot represents an individual mouse, presented as median with interquartile ranges, using a one-way ANOVA with Sidak multiple comparison test.

express low levels of TLR4, whereas TLR4 levels are very low in muscle SCs. Overall, this suggests that both immune and mesenchymal cell populations, which contain the cells-of-origin of NHO,⁽¹⁹⁾ have the potential to respond to LPS in the muscle in vivo.

TLR4 expressed on plasma membrane signals via myddosomes containing MYD88 adaptor protein complexed with IL-1 receptor-activated kinases (IRAK)-1, -2, and -4⁽⁴⁸⁾ to activate NF- κ B transcription factor. In addition, LPS from intracellular bacteria can also be recognized by TLR4 expressed on endosomal membranes. In this case, endosomal TLR4 signals via the adaptor TRIF/TICAM-1 in trifosomes instead of MYD88, to elicit a type I interferon response.^(30,45,49) To elucidate which TLR4 signaling pathway(s) were involved in the exacerbation of NHO after SCI, *Myd88*^{-/-} mice and C57BL/6

controls underwent SCI and intramuscular CDTX together with PBS or LPS at 0.15 mg/kg. Unexpectedly *Myd88*^{-/-} mice showed a trend toward increased NHO bone volumes compared with C57BL/6 mice in the absence of LPS ($p = 0.10$ by ANOVA and $p = 0.025$ by Mann-Whitney). Similar to C57BL/6 mice, LPS treatment resulted in a significant increase in NHO volumes in *Myd88*^{-/-} mice (Fig. 3A, B) and LPS-treated *Myd88*^{-/-} mice also displayed a trend of higher NHO bone volumes compared with LPS-treated C57BL/6 mice, albeit not significant ($p = 0.0549$) (Fig. 3A, B). Next, we examined the development of NHO after SCI in C57BL/6 and *Ticam1*^{-/-} mice. Interestingly, we found that the enhancing effect of LPS on NHO bone volumes was abated in *Ticam1*^{-/-} mice (Fig. 3C, D), demonstrating that LPS exacerbates NHO development via the TRIF/TICAM-1 endosomal route.

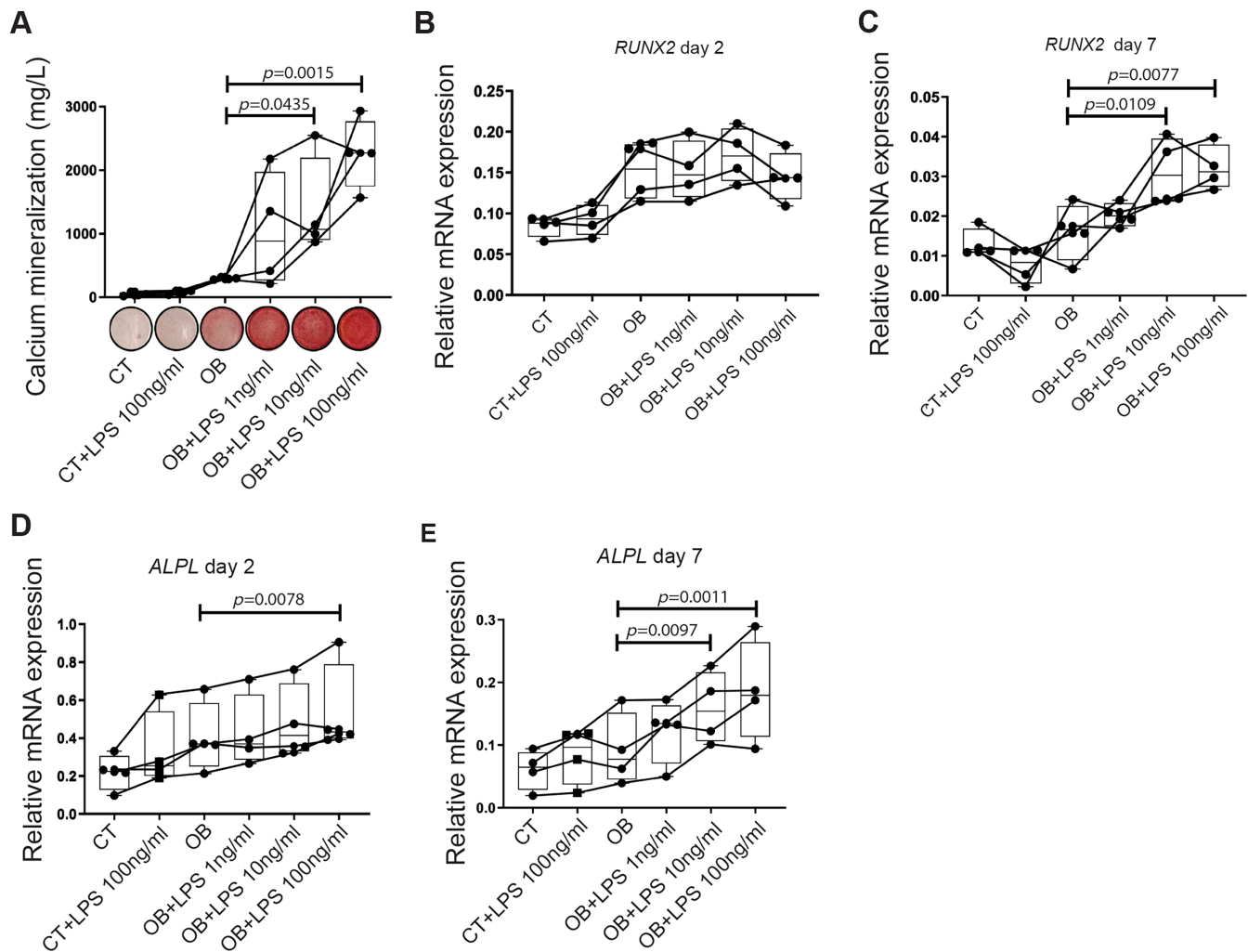


Fig. 5. Lipopolysaccharide (LPS) stimulates calcium mineralization and *RUNX2* and *ALPL* expression of human neurogenic heterotopic ossifications (NHO)-derived fibroadipogenic progenitors (FAPs) in vitro. (A) Dose-response of LPS stimulation (1, 10, and 100 ng/mL) on calcium mineralization of PDGFR α ⁺CD56⁻ FAPs derived from 4 different NHO biopsies/patients cultured in control (CT) or osteogenic medium (OB). After 14 days in culture, mineralization was measured using Alizarin Red staining and quantified. (B–E) Relative expression of *RUNX2* and *ALPL* mRNA levels, measured by RT-qPCR in PDGFR α ⁺CD56⁻ FAPs derived from 4 different NHO biopsies/patients cultured in CT or OB with indicated LPS concentration. RT-qPCR was performed at 2 and 7 days after osteogenic induction. Each line represents results from FAPs purified from the same NHO biopsy/patient; data presented as median with interquartile ranges. Statistical differences were calculated using one-way ANOVA for matched measures with Dunnett's post hoc correction for multiple comparisons.

LPS produced by the gut microflora does not translocate to the circulation after SCI

There are two possible avenues for LPS to enter the body and enhance NHO development: via increased permeability of the gut epithelial barrier or infections (local, distant, or systemic). In respect to the first possibility, it has been reported that SCI at vertebrae T₂ or T₉ leads to gut dysbiosis in mice with increased gut permeability, translocation of bacteria from the gastrointestinal tract into blood, lymph nodes, and spleen together with endotoxemia.⁽⁵⁰⁾ To assess if increased gut permeability was a source of LPS in our NHO mouse model with SCI between T₁₁ to T₁₃, mice underwent Sham or SCI surgery together with CDTX-mediated muscle injury and at 7 days post-surgery, mice were gavaged 4 kDa FITC-dextran, and plasma FITC fluorescence was measured. Naïve mice gavaged FITC-dextran were used as negative controls and mice with dextran sulphate sodium (DSS)-induced colitis were used as positive controls for increased intestinal permeability.⁽⁵¹⁾ SCI and/or CDTX muscle injury did not lead to detectable FITC-dextran leakage into the circulation, whereas FITC-dextran leakage was clearly noted in mice with DSS-induced acute colitis (Fig. 4A). Pathological scoring from similar cohorts of mice showed no significant pathology score increase in small and large intestine of these mice (Fig. 4B–D), which remained low on a 0–14 histopathology score scale.⁽³⁴⁾ We also assessed whether increased bacterial translocation from the gut into the circulation or endotoxemia occurred after SCI and muscle injury (Fig. 4E, F). The 16s prokaryote rRNA gene remained undetectable in the blood of mice from all treatment groups except for DSS-induced colitis positive control (Fig. 4E). Likewise, endotoxin (LPS) plasma concentration remained extremely low with exception of DSS-induced acute colitis mice, which demonstrated clear endotoxemia (Fig. 4F). Thus, we conclude that T₁₁ to T₁₃ SCI and muscle injury does not alter intestinal permeability or cause a detectable endotoxemia or gut bacteria translocation. Thus, LPS leakage from the gut microflora is not necessary to trigger NHO development in our model.

LPS increases osteogenic differentiation of FAPs isolated from muscles surrounding human NHO

As FAPs are the cells-of-origin of NHO in mouse and human muscles⁽¹⁹⁾ and CNS injuries can alter FAP behavior in muscles,⁽⁵²⁾ we sorted PDGFR α ⁺ CD56⁻ FAPs from muscles surrounding NHO biopsies from four different NHO patients (not from healthy donors) to confirm the pro-osteogenic effect of LPS in the human setting. Cells were then cultured in osteogenic conditions with increased doses of LPS. LPS caused a dose-dependent increase in mineral calcium deposition as measured with Alizarin Red (Fig. 5A) and stimulated the expression of *RUNX2* transcripts at day 7 (Fig. 5B, C) and *ALPL* transcripts at day 2 and day 7 (Fig. 5D, E), suggesting FAP osteoblastic differentiation.

NHO prevalence is significantly higher in TBI patients with pseudomonas infections

As the incidence of TBI is higher than that of SCI, we performed a case–control retrospective study on TBI patients to investigate the role of infection and inflammation in NHO development by comparing data from case TBI patients with reported NHO to matched control TBI patients without NHO. A total of 70 TBI patients were admitted to the same ICU and neurorehabilitation department. From this cohort, 6 patients developed NHO (8.6%) (Table 1) typical of reported incidence of NHO in patients suffering TBI at this clinic.

Of the 6 patients who developed NHO, 5 were males (sex ratio: 83.3%). Median age at time of the TBI was 22 years. NHO were located around the hip for 3 patients and at the inner part of the knee for 3 other patients. Diagnosis of NHO was clinically suspected in attendance of joint pain, limitation of range of motion, signs of per-articular inflammations with red, warm, and swollen skin, and confirmed by imaging (X-ray or CT scan).

The remaining 64 patients sustained TBI without developing NHO (53 males; sex ratio: 82.1%). Median age at the time of TBI was 29 years.

No difference was found between case and control groups in term of age, sex, and body mass index. Both groups had a

Table 1. Relationship Between NHO Occurrence and Patients' Characteristics and Circumstances of Head Trauma Analyzed in Univariate Analysis

Variables	Cases (n = 6)	Controls (n = 64)	p Value
Sex ratio, n (%)	5 males (83.3%)	53 males (82.1%)	1.000
Age (years), median [IQR]	22 [20; 29]	29 [22; 40]	0.300
Body mass index (kg/m ²), median [IQR]	25 [23; 26]	23 [21; 26]	0.310
Active smoker, n (%)	2 (33.4%)	24 (37.5%)	1.000
Autoimmune disease, n (%)	0 (0%)	3 (4.7%)	1.000
Addiction (alcohol, cannabis)	2 (33.4%)	13 (20.31%)	0.600
Duration of stay in ICU (days), median [IQR]	31 [27; 46]	17 [9; 29]	0.048
Duration of coma (days), median [IQR]	23 [14; 28]	9 [2; 15]	0.009
Causes of TBI, n (% patient)			0.910
Four-wheel vehicle accident	0 (0%)	11 (17.4%)	
Two-wheel vehicle accident	3 (50%)	19 (30.1%)	
Pedestrian	1 (16.7%)	8 (12.6%)	
Falls	2 (33.3%)	12 (19.1%)	
Other	0 (0%)	14 (21.8%)	
High velocity of the trauma, n (%)	3 (75%)	28 (66.7%)	1.000
Crush-projection of the body during the accident, n (%)	4 (80%)	16 (35.6%)	0.140
Presence of alcohol in the first blood test, n (%)	1 (16.7%)	14 (22.6%)	1.000

Abbreviations: ICU = intensive care unit; IQR = interquartile range; NHO = neurogenic heterotopic ossification; TBI = traumatic brain injury.

Table 2. Relationship Between NHO Occurrence and Infection Variables Analyzed in Univariate Analysis

Variables	Cases (<i>n</i> = 6)	Controls (<i>n</i> = 64)	<i>p</i> Value
Patients with sepsis related to infection, <i>n</i> (%)	6 (100%)	45 (70.3%)	0.180
Patients with septic shock, <i>n</i> (%)	1 (16.7%)	2 (3.1%)	0.240
Patients with pneumonia, <i>n</i> (%)	6 (100%)	44 (68.8%)	0.170
Urinary tract infection, <i>n</i> (%)	2 (33.3%)	2 (3.1%)	0.034
GNB infection, <i>n</i> (%)	6 (100%)	37 (57.8%)	0.075
Enterobacter species	4 (66.7%)	28 (43.8%)	0.400
Pseudomonas species	5 (83.3%)	7 (11.0%)	0.001
Others GNB	2 (33.3%)	24 (37.5%)	1.000
GPC infection, <i>n</i> (%)	3 (50%)	32 (50%)	1.000
Polymicrobial infection, <i>n</i> (%)	6 (100%)	36 (80%)	0.570
Delay from accident to the first infection (days), median [IQR]	4.5 [2.5; 5.8]	5 [3; 6]	0.640
SOFA score, median [IQR]	9.5 [9; 11]	8 [4; 10]	0.140
SAPS II, median [IQR]	45 [34; 52]	34 [26; 49]	0.30

Abbreviations: GNB = gram-negative bacilli; GPC = gram-positive cocci; IQR = interquartile range; NHO = neurogenic heterotopic ossification; SAPS II = Simplified Acute Physiology Score II, min 0–max 100%; SOFA = Sepsis-related Organ Failure Assessment Score, min 0–max 24.

Table 3. Relationship Between NHO Occurrence and Inflammation Variables Analyzed in Univariate Analysis

Themes	Variables	Cases (<i>n</i> = 6)	Controls (<i>n</i> = 64)	<i>p</i> Value
Associated traumas	Bone fracture, <i>n</i> (%)	4 (66.7%)	30 (46.9%)	0.420
	ISS total, median [IQR]	38 [35; 42]	25 [17; 33]	0.007
	AIS Head–neck	5 [5; 5]	4 [3; 5]	0.031
	AIS Face	0 [0; 0]	0 [0; 1]	0.081
	AIS Chest	2.5 [0.5; 3]	2 [0; 3]	0.490
	AIS Pelvis–abdomen	2 [0.5; 2.8]	0 [0; 0]	0.012
	AIS Limbs	2 [2; 2.8]	0 [0; 2]	0.074
	Surgery or drain implantation total, <i>n</i> (%)	6 (100%)	35 (54.7%)	0.038
	Bone fracture	5 (83.3%)	15 (23.4%)	0.006
	Chest–pelvis–abdominal trauma	3 (50%)	9 (14.1%)	0.050
Craniectomy, craniotomy and extracranial derivation	4 (66.7%)	22 (34.4%)	0.190	
Neurology	Glasgow Coma scale, median [IQR]	6 [4.5; 6.8]	7.5 [4.8; 12]	0.250
	Focal intracranial lesions on first CT scan, <i>n</i> (%)	4 (66.7%)	51 (79.7%)	0.600
	Diffuse intracranial lesions on first CT scan, <i>n</i> (%)	6 (100%)	55 (85.9%)	1.000
	Intracranial hypertension >25 mmHg, <i>n</i> (%)	4 (66.7%)	25 (47.2%)	0.420
	Cognitive disorder at discharge from ICU, <i>n</i> (%)	6 (100%)	52 (81.3%)	0.580
	Motor deficiency at discharge from ICU, <i>n</i> (%) patient	4 (66.7%)	24 (37.5%)	0.210
Respiratory	Duration of oro-tracheal intubation (days), median [IQR]	36 [24; 54]	15 [10; 20]	0.001
	Duration of mechanic ventilation (days), median [IQR]	32 [26; 54]	15 [10; 22]	0.001
	Implantation of tracheotomy, <i>n</i> (%)	5 (83.3%)	17 (26.6%)	0.010
Drugs	Acute respiratory distress syndrome, <i>n</i> (%)	4 (66.7%)	16 (27.6%)	0.071
	Medications for sedation, median [IQR]	3.5 [2.2; 4]	2 [2; 3]	0.130
	Length of sedation (days), median [IQR]	7.5 [4.5; 19]	6 [2; 12]	0.190
	Use of curare >24 hours, <i>n</i> (%)	3 (50%)	16 (25%)	0.330
	Use of vasoplegic drugs >24 hours, <i>n</i> (%)	6 (100%)	45 (70.3%)	0.180
Complications	Use of corticoids, <i>n</i> (%)	1 (20%)	13 (21.0%)	1.000
	Bedsore, <i>n</i> (%) patient	0 (0%)	5 (7.8%)	1.000
	Vein thrombosis, <i>n</i> (%) patient	2 (33.3%)	5 (7.8%)	0.110
Chronic inflammatory disease	Diabetes type 1 and 2, <i>n</i> (%) patient	0 (0%)	0 (0%)	1.000
	Autoimmune diseases, <i>n</i> (%) patient	0 (0%)	3 (4.69%)	1.000
	Metabolic syndrome, <i>n</i> (%) patient	0 (0%)	0 (0%)	1.000

Note: Bold indicates statistically significant value ($p < 0.05$).

Abbreviations: AIS = Abbreviated Injury Scale, min 1–max 6; ISS = Injury Severity Score, min 0–max 75; IQR = interquartile range; NHO = neurogenic heterotopic ossification.

similar medical history regarding percentage of active smokers, autoimmune disease, and addiction to alcohol and cannabis (Table 1).

The duration of stay in ICU was significantly prolonged in patients with NHO compared with patients without NHO (31 versus 7 days, $p = 0.048$). The duration of coma was twice longer in

the population with NHO relative to patients without NHO ($p = 0.009$).

We found no difference between cases and controls in term of etiologies of TBI, high velocity of the trauma, crush-projection of the body during the accident, and presence of alcohol in the first blood test.

Patients who developed NHO all presented sepsis-related infections during ICU hospitalization compared with controls (Table 2). Urinary tract infections occurred significantly more frequently in cases involving the development of NHO ($p = 0.034$). Pneumonia acquired under mechanical ventilation happened in all patients with NHO, but no statistical difference was detected compared with the control group ($p = 0.075$). Infections with gram-negative bacteria (GNB) were diagnosed in 100% of patients who developed NHO versus 57.8% of patients without NHO. However, this did not reach significance ($p = 0.075$). *Pseudomonas aeruginosa* were more commonly associated with NHO-developing patients (83.3%) than patients who did not develop NHO (11.0%, $p = 0.034$), suggesting a significant association between the development of NHO and septic infection during intensive care with gram-negative bacterium *Pseudomonas aeruginosa*.

Associated traumas, including bone fracture and chest-pelvis-abdominal traumas, were more frequent in the group with NHO (66.7% and 83.3%, respectively) than in the group without NHO (46.9% and 53.1%, respectively) but statistical analysis found no difference (Table 3). In contrast, total injury severity score (ISS) was 13 points higher in patients with NHO formation in comparison with patients with no NHO ($p = 0.007$). Surgeries or drain implantations for an associated trauma were significantly more frequent in patients who developed NHO compared with patients who did not develop NHO ($p = 0.038$). These results indicate that surgeries, drain implantations, and ISS after TBI are associated with NHO formation.

For all neurogenic variables, we found no significant difference between the two groups of patients. Our results suggested that both populations are quite similar in terms of neurological presentation and variables related did not seem to impact NHO development.

Oro-tracheal extubation was performed twice later on a patient who developed NHO in contrast with a patient who had no NHO (36 versus 15 days post-injury, $p = 0.001$). The need of mechanical ventilator support was longer for patients with NHO in comparison with patients without NHO (32 versus 15 days, $p = 0.001$). We found a higher incidence of tracheotomy in the group that develop NHO compared with the group that did not develop NHO ($p = 0.01$). Although acute respiratory distress syndrome was twice more frequent in cases compared with controls, the difference between both groups was not significant.

Medications and duration of sedation were comparable between the two groups. Interestingly, curare and vasoplegic drugs (adrenalin and noradrenalin) were more prescribed in population of patients with NHO (50% and 100%, respectively) in comparison with population of patients without NHO (25% and 70.3%, respectively). We found no difference between the two groups of patients in terms of SOFA score, SAPS II, bedsores, and deep vein thrombosis.

Finally, very few patients had chronic inflammatory, autoimmune diseases, or metabolic syndromes that may have influenced NHO development and progression (Table 3). Presence/absence of inflammatory bowel disease was not recorded in the patients' database.

Discussion

Previous retrospective studies in victims of SCI or TBI have shown a significantly higher incidence of NHO in patients with systemic infections, urinary tract infections, or pneumonia.^(4,13-16) However, these studies did not determine whether mechanistically, infectious pathogens are the direct cause of enhanced incidence of NHO or a mere reflection of the immunodepression subsequent to severe TBI and high-level SCI.^(53,54) Indeed, severe TBI and high-level SCI can disrupt the central control of the sympathetic nervous system and the neuroendocrine complex. Loss of central control of sympathetic innervation of lymphoid organs and adrenal glands can lead to lymphopenia and immunodepression.⁽⁵³⁻⁵⁵⁾ In our model, the spinal cord is trans-sectioned at relatively low levels between vertebrae T₁₁ to T₁₃ below the preganglionic neurons controlling sympathetic neurons innervating the spleen⁽⁵⁶⁾ and does not cause autonomic dysreflexia, which in itself causes a regression of lymphoid organs and immunodepression.⁽⁵⁵⁾

We demonstrate in our mouse model that local or systemic administration of LPS exacerbates NHO development via the LPS receptor TLR4 and the endosomal TRIF pathway, not via the MYD88 pathway from extracellular LPS (summarized in Fig. 6). Interestingly, we saw a trend toward increased NHO bone volumes in *Myd88*^{-/-} compared with C57BL/6 controls both in the presence and absence of LPS. MYD88 is a key adaptor protein in signaling mediated by the IL-1 receptor and toll-like receptors expressed on the plasma membrane (TLR1/TLR2, TLR2/6, TLR4, TLR5), as well TLRs expressed on endosomal surfaces (TLR7, TLR9). MYD88 is also important in regulating myoblast fusion as *Myd88* gene deletion inhibits postnatal muscle growth.⁽⁵⁷⁾ Whether the regeneration potential of satellite cells post-SCI and muscle injury was impacted and favored NHO development in *Myd88*^{-/-} mice remains to be investigated. We also hypothesized that this trend toward increased NHO in *Myd88*^{-/-} mice was due to TLR4 signaling being rerouted toward TRIF/TICAM-1. In support of this interpretation, we found that NHO bone volumes were abated in *Ticam1*^{-/-} mice in the presence of LPS.

As TLR4 was expressed by both mesenchymal FAPs and monocytes/macrophages in muscles, the effect of LPS on NHO development could have contributions from both myeloid and mesenchymal cells. Whether FAPs and myeloid cells both respond to LPS after SCI and muscle injury was not investigated in mice; however, future experiments with conditional deletion of the *Tlr4* gene in FAPs (eg, using *Pdgfra*-Cre or *Prrx1*-Cre mice) or in myeloid cells (eg, with *Lyz2*-Cre mice) would clarify this. Nevertheless, in vitro administration of LPS to human FAPs purified from muscles surrounding NHO biopsies resulted in increased calcium mineralization in a dose-dependent manner and expression of maturing osteoblast genes *RUNX2* and *ALPL*, thus suggesting that LPS has the potential to directly activate an osteoblastic program in FAPs. We have also previously shown that medium conditioned by LPS-activated human monocytes increases mineralization and expression of osteoblast genes in FAPs isolated from muscles surrounding NHO biopsies.⁽²³⁾ This suggests that in humans, LPS may increase NHO formation both directly by stimulating an osteogenic program in muscle FAPs, and indirectly via macrophages infiltrating injured muscles.

Importantly, we find that intramuscular LPS injection did not alter myeloid cell recruitment to the CDTX-injured muscle. However, LPS administration caused an early burst of mRNA encoding OSM, IL-1 α , and IL-1 β in injured muscles, cytokines we have

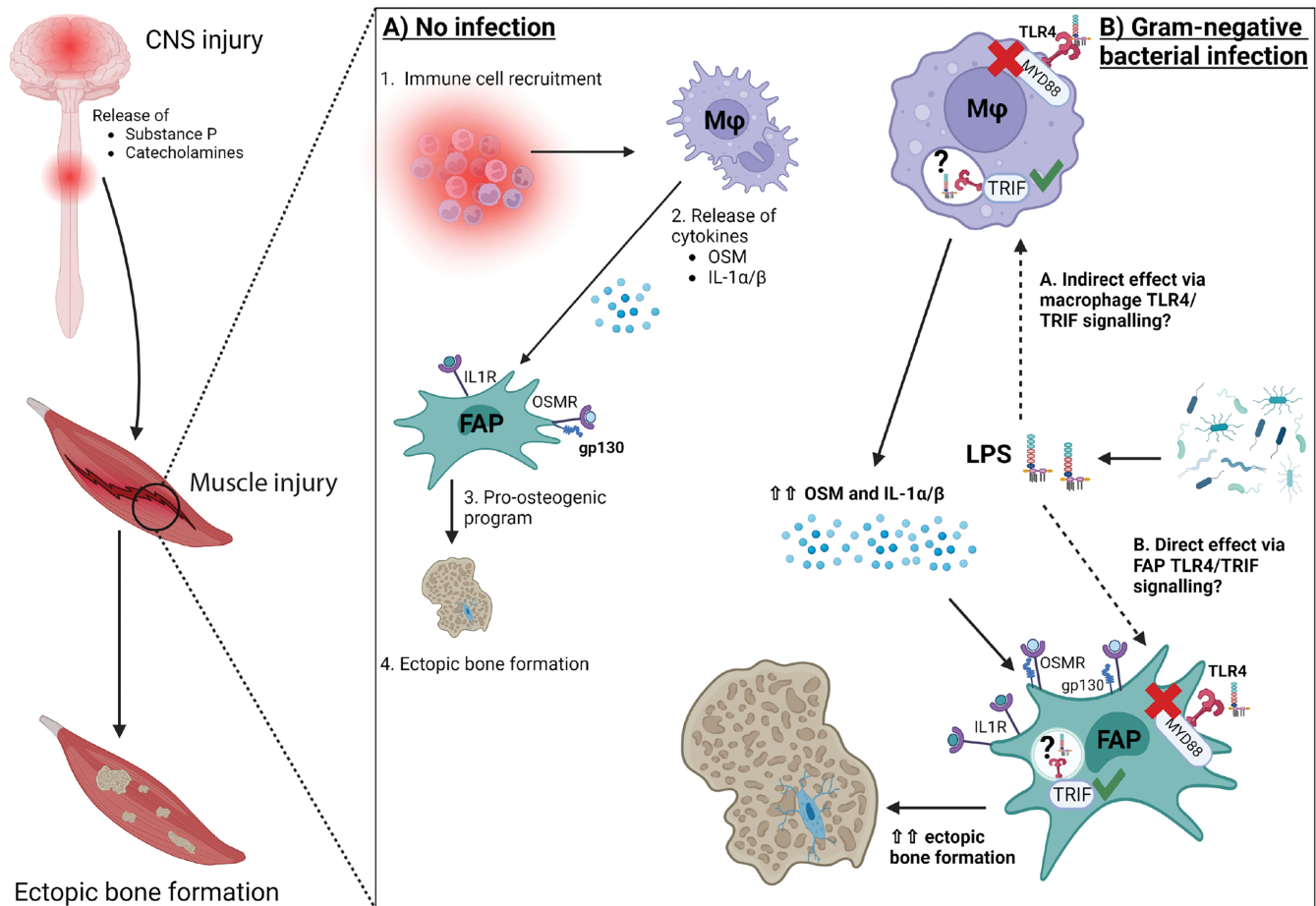


Fig. 6. Model of lipopolysaccharide (LPS) action on neurogenic heterotopic ossifications (NHO) development. A dual insult to the central nervous system (CNS; spinal cord injury [SCI] or traumatic brain injury [TBI]) combined with muscle injury leads to the development of NHO in the injured muscle. We have previously shown that the CNS injury triggers the release of neuro-endocrine mediators such as catecholamines and the neuropeptide substance P, which promote NHO development.^(17,18) (A) In the absence of infection: (1) Inflammatory macrophages are recruited to the site of injury, (2) with enhanced release of pro-inflammatory cytokines OSM and IL-1 α/β under the effect of neuro-endocrine stimulators; this (3) drives a pro-osteogenic program in FAPs, which are the cells-of-origin of NHO, which subsequently differentiate into osteoblasts and deposit ectopic bone. (B) However, in the presence of an infection from gram-negative bacteria, LPS is released, which has the potential (dotted arrows) to exacerbate NHO development in a TRIF-dependent manner (a) indirectly via TLR4/TRIF-mediated signaling in macrophages, which further increase OSM and IL-1 α/β release, or (b) directly via TLR4/TRIF-mediated signaling in FAPs, or both. Image created with [BioRender.com](https://www.biorender.com).

previously shown to functionally contribute to NHO development in response to SCI.^(22,23) However, this earlier burst of cytokine mRNA expression did not accelerate NHO development as NHO develops as early as day 5 in mice with or without LPS treatment. Instead, mineralization was amplified by administration of LPS.

Our data illustrating the role of LPS exacerbating NHO bone formation is consistent with other studies investigating infection in animal models of trauma-induced heterotopic ossification (HO). In a rat traumatic blast HO model, the presence of bioburden (*Acinetobacter* and methicillin-resistant *Staphylococcus aureus*) significantly increased ectopic bone formation and a short-term treatment with vancomycin attenuated HO formation.⁽⁵⁸⁾

Our and these findings are in sharp contrast to two recent reports in a model of HO driven by implantation of skin fibroblasts transduced with an adenovirus to overexpress mouse

bone morphogenetic protein (BMP)-2 or collagen sponge impregnated with recombinant BMP-2, which both showed that LPS treatment decreased HO development *in vivo*.^(59,60) It must be noted, however, that supraphysiological BMP-2 overexpression is nonphysiological, very osteogenic, and this does not represent a physiologically relevant model of SCI-induced NHO.^(12,19) Furthermore, LPS-activated mouse macrophages express *Acvr1* and *Acvr2a* mRNA (see www.biogps.org), which encode BMP receptors, and this may alter their subsequent response to LPS once stimulated by supraphysiological concentrations of BMP-2. Therefore, it is difficult to extrapolate from these studies in which BMP-2 is artificially overexpressed, the relevance to SCI-induced NHO that does not involve supraphysiological expression of BMP-2 in the muscle.⁽¹⁹⁾ On the other hand, our results clearly suggest that LPS polarizes muscle-infiltrating macrophages *in vivo* in ways that enhance NHO development with increased expression of OSM, IL-1 α , and IL-1 β , which we

have previously shown to functionally contribute to NHO development.^(22,23)

Interestingly, the anabolic effect of LPS in our model of SCI-induced intramuscular NHO is in contrast to other reports showing that (i) chronic LPS administration in mice leads to skeletal bone loss, mostly by increasing osteoclastogenesis as recently reviewed in a meta-analysis,⁽⁶¹⁾ and (ii) that addition of LPS in cultures of the mouse pro-osteoblastic immortalized cell line MC3T3-E1⁽⁶²⁾ or primary calvarial osteoblasts⁽⁶³⁾ reduces expression of osteoblast markers. However, a number of articles have also shown that LPS can have an anabolic effect on mesenchymal progenitor cells isolated from human bone marrow,⁽⁶⁴⁾ umbilical cord blood,⁽⁶⁵⁾ periodontal ligaments,⁽⁶⁶⁾ mouse bone marrow,⁽⁶⁷⁾ and increases expression of osteoblast markers and mineralization. Therefore, the effect of LPS may vary depending on the tissue of origin of mesenchymal progenitor cells. This is consistent with previous observations that mesenchymal progenitor cells isolated from very different tissues (eg, from muscle versus periosteum) have very different differentiation potential in vivo.⁽⁶⁸⁾

LPS is restricted to gram-negative bacteria, which can enter the body through a local infection or via the circulation. Several reports have highlighted gut dysbiosis after SCI in humans and mice (reviewed in Valido and colleagues⁽⁶⁹⁾ and Jogia and Ruitenberg⁽⁷⁰⁾), with the potential of increased intestinal permeability of gut microflora, which contain gram-negative bacteria such as Bacteroidetes and Proteobacteria,⁽⁷¹⁾ which comprises *E. coli* and *Pseudomonas* species. One study reported that mice with a T₂ or T₉ contusion had increased intestinal permeability with bacteria translocation to lungs, spleens, and lymph nodes and endotoxemia.⁽⁵⁰⁾ Using a raft of assays to measure gut permeability after oral gavage with fluorescent FITC-dextran, gut histopathology scoring, endotoxemia, and blood bacterial load by PCR for the 16s prokaryotic rRNA gene, we could not detect any increase of these parameters in mice with SCI between T₁₁ and T₁₃ in contrast to this previous report.⁽⁵⁰⁾ As we did not perform a transection at the same thoracic level at this study, it is possible that changes in gut dysbiosis and intestinal permeability are lesion-level dependent. However, we can conclude that in our model with complete transection of the spinal cord between T₁₁ and T₁₃, increased intestinal permeability and endotoxemia are not the driving force of and are not necessary for NHO development. Together, these results suggest that infections with exogenous gram-negative bacteria may be an important factor contributing to NHO development.

Finally, we performed a retrospective control–case study on 70 victims of severe TBI all treated at that same ICU and followed in the same rehabilitation center, which, to our knowledge, is the first detailing infectious and inflammatory features that occur early after TBI and their relationship with NHO development. We also provided evidence that involvement of gram-negative bacteria infections, and more specifically *Pseudomonas aeruginosa*, are significantly associated. A total of 83% TBI patients with NHO had experienced a *Pseudomonas* infection, whereas only 11% of TBI patients without NHO had such infection. Why 7 of 70 (10%) TBI patients did not develop NHO despite experiencing a *Pseudomonas* infection remains to be determined as the time of infection relative to TBI did not seem to influence the occurrence or absence of NHO.

It was also noted that patients with severe TBI did not systematically develop NHO. Therefore, we propose that TBI predisposes patients to NHO by increasing the systemic level of inflammation, similar to the effect of SCI on the inflammatory

response in injured muscles in mice,^(22–24) but a higher level of inflammation or muscle injury threshold is required to initiate NHO. Similar to HO encountered in non-neurogenic pathologies (burns, amputation, Guillain–Barre syndrome, long stay in ICU), we found that surgeries, associated trauma, and infections are significantly associated with NHO production, probably because they drive more inflammation. Infection has also been shown to be associated with the development of acquired HO in patients with severe burns,^(72,73) traumatic and combat-related injuries,⁽⁷⁴⁾ and hip arthropathy.^(75,76) Thus, we hypothesize that NHO needs a certain inflammatory threshold to induce ossification of muscle progenitor cells soon after the initial trauma. Patients with CNS damage who are hospitalized in ICU for vital care are more likely to develop infections, especially patients with severe TBI and a Glasgow coma score <8.^(77,78) The type of neurological lesion influences the bacterial infections that occur within patients. This can be observed in SCI patients who suffer from bladder dysfunction, which often leads to urinary tract infections.⁽⁷⁹⁾ On the other hand, TBI can be responsible for swallowing deficiency and may also cause lung infections.⁽⁸⁰⁾ Infections, and more specifically pneumonia and urinary tract infections, have been reported in the literature as risk factors of NHO development after SCI^(14,16) and TBI.^(3,4) We also identified a higher incidence of urinary tract infections in patients who developed NHO. In contrast, pneumonia occurrence was not significantly different between the groups, although 100% of patients who developed NHO experienced at least one episode of pneumonia during their stay in ICU. The number of sepsis related to infection during ICU stay was not correlated with NHO occurrence, but all patients who developed NHO had one or more septic infections. Thus, our study does support the link between infection, and more specifically urinary tract infections, with NHO development.

The main limitation of this case–control correlative study is its small size, which was due to the rigorous restrictive selection process to ensure that all patients involved in this retrospective study were recruited after receiving treatment in the same ICU and neuro-rehabilitation departments, with homogenous patient cohorts in respect to their neurological status. Therefore, the low number of TBI patients with NHO ($n = 6$) limited the statistical analysis power of the study, particularly in respect to infections with gram-negative bacteria and pneumonia (both with p value of 0.075), and the ability to perform multivariate analysis. Nevertheless, this study is the first to document in victims of TBI a significant association between incidence of NHO and infections with gram-negative *Pseudomonas aeruginosa* and to provide mechanistic insights demonstrating in a mouse model of SCI-induced NHO that LPS produced by gram-negative bacteria exacerbates NHO development in injured muscles.

Our work suggests that pharmacological compounds targeting the TLR4/TRIF pathway may be beneficial to reduce NHO incidence in SCI/TBI patients. However, the only known cell-permeable selective TRIF inhibitor is the fusion peptide pepinh-TRIF. To our knowledge, this compound has not been tested in vivo. General inhibition of endotoxins (eg, by hemoperfusion through polymyxin B loaded cartridges as free polymyxin B is nephrotoxic and neurotoxic), TLR4/MD2 antagonists (eg, eritoran), or general TLR4 signaling inhibitors (eg, resatovid) have shown limited efficacy in clinical trials on patients with severe sepsis.^(81–83) Although these pharmacological treatments may be beneficial to reduce NHO incidence in victims of TBI/SCI, the best strategy forward until these drugs are trialed for their efficacy to mitigate NHO is, in our opinion, to employ utmost aseptic

procedures and environment and increase microbe vigilance and prophylaxis, to reduce incidence of NHO in victims of SCI and TBI. Further retrospective and prospective studies to link specific gram-negative and gram-positive infections with NHO incidence in larger cohorts of SCI and TBI patients are warranted.

Author Contributions

Marjorie Salga: Conceptualization; methodology; investigation; writing – original draft; writing – review and editing; formal analysis; project administration. **Selwin G. Samuel:** Investigation; writing – original draft; formal analysis. **Hsu-Wen Tseng:** Investigation; writing – original draft; formal analysis. **Laure Gatineau:** Investigation; formal analysis; data curation. **Dorothee Girard:** Investigation; writing – original draft; formal analysis; conceptualization. **Bastien Rival:** Investigation; formal analysis. **Valerie Barbier:** Investigation; formal analysis. **Kavita Bisht:** Investigation; formal analysis. **Svetlana Shatunova:** Investigation; formal analysis. **Charlotte Debaud:** Investigation. **Ingrid G. Winkler:** Writing – review and editing. **Julie Paquereau:** Investigation; formal analysis. **Aurélien Dinh:** Investigation; formal analysis. **Guillaume Genêt:** Data curation; formal analysis. **Sébastien Ker-ever:** Investigation; formal analysis. **Paer-Sélim Abback:** Investigation; formal analysis. **Sébastien Banzet:** Conceptualization; methodology; funding acquisition; writing – original draft; writing – review and editing; supervision; resources. **François Genêt:** Methodology; supervision; conceptualization; project administration; resources. **Jean-Pierre Lévesque:** Conceptualization; methodology; funding acquisition; writing – original draft; writing – review and editing; supervision; resources; project administration. **Kylie A. Alexander:** Investigation; formal analysis; supervision; writing – review and editing; writing – original draft; conceptualization.

Acknowledgments

This work was part of MS's and SGS's PhD theses. We thank Prof Marc Ruitenbergh and Dr Ran Wan for helpful discussions and Dr Seungha Kang, Ms Lauren Schooth, and Mr Muhammed Sabdia for helping with 16s rRNA detection. We thank the Translational Research Institute histology, flow cytometry, and preclinical imaging facilities and The University of Queensland Biological Resources Facility. This work was initially supported by award W81XWH-15-1-0606 from the Congressionally Approved Spinal Cord Injury Research Program of the US Department of Defense (JPL and FG), then by an Ideas Grant 1181053 from the National Health and Medical Research Council of Australia (NHMRC) to JPL, KAA, HT, SB, and FG, and by the Mater Foundation. SB was also supported by BIOMEDEF SAN-1-2209 from the French Government Defense procurement and technology agency (Direction Générale de l'Armement DGA). KB is supported by an American Society of Hematology Global Research Award and LINC grant awarded by TRI and Metro South Health/Mater. JPL was supported by Research Fellowship 1136130 from the NHMRC. SGS and SS were supported by International Scholarship from the University of Queensland and MS by ORPEA-CLINEA company and grant from the Collège Français des Enseignants Universitaires de Médecine Physique et de Réadaptation (COFEMER). Open access publishing facilitated by The University of Queensland, as part of the Wiley - The University of Queensland agreement via the Council of Australian University Librarians.

Disclosures

The authors have declared that no conflicts of interest exist.

Peer Review

The peer review history for this article is available at <https://www.webofscience.com/api/gateway/wos/peer-review/10.1002/jbmr.4905>.

Data Availability Statement

The data that support the findings of this study are available from the corresponding author upon reasonable request.

References

- Genet F, Jourdan C, Schnitzler A, et al. Troublesome heterotopic ossification after central nervous system damage: a survey of 570 surgeries. *PLoS One*. 2011;6(1):e16632.
- van Kuijk AA, Geurts AC, van Kuppevelt HJ. Neurogenic heterotopic ossification in spinal cord injury. *Spinal Cord*. 2002;40(7):313–326.
- Dizdar D, Tiftik T, Kara M, et al. Risk factors for developing heterotopic ossification in patients with traumatic brain injury. *Brain Inj*. 2013;27(7–8):807–811.
- Reznik JE, Biros E, Marshall R, et al. Prevalence and risk-factors of neurogenic heterotopic ossification in traumatic spinal cord and traumatic brain injured patients admitted to specialised units in Australia. *J Musculoskelet Neuronal Interact*. 2014;14(1):19–28.
- Garland DE, Orwin JF. Resection of heterotopic ossification in patients with spinal cord injuries. *Clin Orthop Relat Res*. 1989;242:169–176.
- Vanden Bossche L, Vanderstraeten G. Heterotopic ossification: a review. *J Rehabil Med*. 2005;37(3):129–136.
- Genet F, Chehensse C, Jourdan C, et al. Impact of the operative delay and the degree of neurologic sequelae on recurrence of excised heterotopic ossification in patients with traumatic brain injury. *J Head Trauma Rehabil*. 2012;27(6):443–448.
- Genet F, Marmorat JL, Lauridou C, et al. Impact of late surgical intervention on heterotopic ossification of the hip after traumatic neurological injury. *J Bone Jt Surg Br*. 2009;91(11):1493–1498.
- Genêt F, Minooee K, Jourdan C, et al. Troublesome heterotopic ossification and stroke: features and risk factors. A case control study. *Brain Inj*. 2018;29(7–8):866–871.
- Ohlmeier M, Suero EM, Aach M, et al. Muscle localization of heterotopic ossification following spinal cord injury. *Spine J*. 2017;17(10):1519–1522.
- Almangour W, Schnitzler A, Salga M, et al. Recurrence of heterotopic ossification after removal in patients with traumatic brain injury: a systematic review. *Ann Phys Rehabil Med*. 2016;59(4):263–269.
- Alexander KA, Tseng H-W, Salga M, Genêt F, Levesque J-P. When the nervous system turns skeletal muscles into bones: how to solve the conundrum of neurogenic heterotopic ossification. *Curr Osteoporos Rep*. 2020;18(6):666–676.
- Hendricks HT, Geurts AC, van Ginneken BC, Heeren AJ, Vos PE. Brain injury severity and autonomic dysregulation accurately predict heterotopic ossification in patients with traumatic brain injury. *Clin Rehabil*. 2007;21(6):545–553.
- Citak M, Suero EM, Backhaus M, et al. Risk factors for heterotopic ossification in patients with spinal cord injury: a case-control study of 264 patients. *Spine*. 2012;37(23):1953–1957.
- van Kampen PJ, Martina JD, Vos PE, Hoedemaekers CW, Hendricks HT. Potential risk factors for developing heterotopic ossification in patients with severe traumatic brain injury. *J Head Trauma Rehabil*. 2011;26(5):384–391.

16. Suero EM, Meindl R, Schildhauer TA, Citak M. Clinical prediction rule for heterotopic ossification of the hip in patients with spinal cord injury. *Spine*. 2018;43(22):1572–1578.
17. Genêt F, Kulina I, Vaquette C, et al. Neurological heterotopic ossification following spinal cord injury is triggered by macrophage-mediated inflammation in muscle. *J Pathol*. 2015;236(2):229–240.
18. Debaud C, Tseng H-W, Chedik M, et al. Local and systemic factors drive ectopic osteogenesis in regenerating muscles of spinal cord-injured mice in a lesion level-dependent manner. *J Neurotrauma*. 2021;38(15):2162–2175.
19. Tseng H-W, Girard D, Alexander KA, et al. Spinal cord injury reprograms muscle fibroadipogenic progenitors to form heterotopic bones within muscles. *Bone Res*. 2022;10(1):22.
20. Alexander KA, Tseng H-W, Kulina I, et al. Lymphocytes are not required for neurogenic heterotopic ossification development after spinal cord injury. *Neurotrauma Rep*. 2022;3(1):87–96.
21. Tseng H-W, Kulina I, Salga M, et al. Neurogenic heterotopic ossifications develop independently of granulocyte colony-stimulating factor and neutrophils. *J Bone Miner Res*. 2020;35(11):2242–2251.
22. Tseng H-W, Kulina I, Girard D, et al. Interleukin-1 is overexpressed in injured muscles following spinal cord injury and promotes neurogenic heterotopic ossification. *J Bone Miner Res*. 2022;37(3):531–546.
23. Torossian F, Guerton B, Anginot A, et al. Macrophage-derived oncostatin M contributes to human and mouse neurogenic heterotopic ossifications. *JCI Insight*. 2017;2(21):e96034.
24. Alexander KA, Tseng H-W, Fleming W, et al. Inhibition of JAK1/2 tyrosine kinases reduces neurogenic heterotopic ossification after spinal cord injury. *Front Immunol*. 2019;10:377.
25. Dinarello CA, Simon A, van der Meer JWM. Treating inflammation by blocking interleukin-1 in a broad spectrum of diseases. *Nat Rev Drug Discovery*. 2012;11(8):633–652.
26. Gong Y, Yan X, Sun X, et al. Oncostatin M is a prognostic biomarker and inflammatory mediator for sepsis. *J Infect Dis*. 2020;221(12):1989–1998.
27. Salim SY, AlMalki N, Macala KF, et al. Oncostatin M receptor type II knockout mitigates inflammation and improves survival from sepsis in mice. *Biomedicine*. 2023;11(2):483.
28. Hoshino K, Takeuchi O, Kawai T, et al. Toll-like receptor 4 (Tlr4)-deficient mice are hyporesponsive to lipopolysaccharide: evidence for Tlr4 as the *Lps* gene product. *J Immunol*. 1999;162(7):3749–3752.
29. Adachi O, Kawai T, Takeda K, et al. Targeted disruption of the MyD88 gene results in loss of IL-1- and IL-18-mediated function. *Immunity*. 1998;9(1):143–150.
30. Yamamoto M, Sato S, Hemmi H, et al. Role of adaptor TRIF in the MyD88-independent toll-like receptor signaling pathway. *Science*. 2003;301(5633):640–643.
31. Lilley E, Andrews MR, Bradbury EJ, et al. Refining rodent models of spinal cord injury. *Exp Neurol*. 2020;328:113273.
32. Kitajima S, Takuma S, Morimoto M. Histological analysis of murine colitis induced by dextran sulfate sodium of different molecular weights. *Exp Anim*. 2000;49(1):9–15.
33. Perse M, Cerar A. Dextran sodium sulphate colitis mouse model: traps and tricks. *J Biomed Biotechnol*. 2012;2012:718617.
34. Erben U, Lodenkemper C, Doerfel K, et al. A guide to histomorphological evaluation of intestinal inflammation in mouse models. *Int J Clin Exp Pathol*. 2014;7(8):4557–4576.
35. Breslow N. Design and analysis of case-control studies. *Annu Rev Public Health*. 1982;3:29–54.
36. Seymour CW, Liu VX, Iwashyna TJ, et al. Assessment of clinical criteria for sepsis: for the Third International Consensus Definitions for Sepsis and Septic Shock (Sepsis-3). *JAMA*. 2016;315(8):762–774.
37. Shankar-Hari M, Phillips GS, Levy ML, et al. Developing a new definition and assessing new clinical criteria for septic shock: for the Third International Consensus Definitions for Sepsis and Septic Shock (Sepsis-3). *JAMA*. 2016;315(8):775–787.
38. Baker SP, O'Neill B, Haddon W Jr, Long WB. The injury severity score: a method for describing patients with multiple injuries and evaluating emergency care. *J Trauma*. 1974;14(3):187–196.
39. Vincent JL, Sakr Y, Sprung CL, et al. Sepsis in European intensive care units: results of the SOAP study. *Crit Care Med*. 2006;34(2):344–353.
40. Vincent J-L, Rello J, Marshall J, et al. International study of the prevalence and outcomes of infection in intensive care units. *JAMA*. 2009;302(21):2323–2329.
41. Le Gall JR, Lemeshow S, Saulnier F. A new simplified acute physiology score (SAPS II) based on a European/North American multicenter study. *JAMA*. 1993;270(24):2957–2963.
42. Fink MP. Animal models of sepsis. *Virulence*. 2014;5(1):143–153.
43. Tateda K, Matsumoto T, Miyazaki S, Yamaguchi K. Lipopolysaccharide-induced lethality and cytokine production in aged mice. *Infect Immun*. 1996;64(3):769–774.
44. Nagai Y, Akashi S, Nagafuku M, et al. Essential role of MD-2 in LPS responsiveness and TLR4 distribution. *Nat Immunol*. 2002;3(7):667–672.
45. Shibata T, Motoi Y, Tanimura N, et al. Intracellular TLR4/MD-2 in macrophages senses gram-negative bacteria and induces a unique set of LPS-dependent genes. *Int Immunol*. 2011;23(8):503–510.
46. Zeuner M, Bieback K, Wiedera D. Controversial role of toll-like receptor 4 in adult stem cells. *Stem Cell Rev Rep*. 2015;11(4):621–634.
47. Sambasivan R, Yao R, Kissenpfennig A, et al. Pax7-expressing satellite cells are indispensable for adult skeletal muscle regeneration. *Development*. 2011;138(17):3647–3656.
48. Moncrieffe MC, Bollschweiler D, Li B, et al. Myd88 death-domain oligomerization determines myddosome architecture: implications for toll-like receptor signaling. *Structure*. 2020;28(3):281–289.e3.
49. Bryant CE, Symmons M, Gay NJ. Toll-like receptor signalling through macromolecular protein complexes. *Mol Immunol*. 2015;63(2):162–165.
50. Kigerl KA, Hall JCE, Wang L, et al. Gut dysbiosis impairs recovery after spinal cord injury. *J Exp Med*. 2016;213(12):2603–2620.
51. Yan Y, Kolachala V, Dalmasso G, et al. Temporal and spatial analysis of clinical and molecular parameters in dextran sodium sulfate induced colitis. *PLoS One*. 2009;4(6):e6073.
52. Madaro L, Passafaro M, Sala D, et al. Denervation-activated STAT3–IL-6 signalling in fibro-adipogenic progenitors promotes myofibres atrophy and fibrosis. *Nat Cell Biol*. 2018;20(8):917–927.
53. Meisel C, Schwab JM, Prass K, Meisel A, Dirnagl U. Central nervous system injury-induced immune deficiency syndrome. *Nat Rev Neurosci*. 2005;6(10):775–786.
54. Held KS, Lane TE. Spinal cord injury, immunodepression, and antigenic challenge. *Semin Immunol*. 2014;26(5):415–420.
55. Zhang Y, Guan Z, Reader B, et al. Autonomic dysreflexia causes chronic immune suppression after spinal cord injury. *J Neurosci*. 2013;33(32):12970–12981.
56. Jung W-C, Levesque J-P, Ruitenberg MJ. It takes nerve to fight back: the significance of neural innervation of the bone marrow and spleen for immune function. *Semin Cell Dev Biol*. 2017;61:60–70.
57. Hindi SM, Shin J, Gallot YS, et al. MyD88 promotes myoblast fusion in a cell-autonomous manner. *Nat Commun*. 2017;8(1):1624.
58. Pavay GJ, Qureshi AT, Hope DN, et al. Bioburden increases heterotopic ossification formation in an established rat model. *Clin Orthop Relat Res*. 2015;473(9):2840–2847.
59. Olmsted-Davis E, Mejia J, Salisbury E, Gugala Z, Davis AR. A population of M2 macrophages associated with bone formation. *Front Immunol*. 2021;12:686769.
60. Matsumoto A, Takami M, Urano E, et al. Lipopolysaccharide (LPS) inhibits ectopic bone formation induced by bone morphogenetic protein-2 and TGF- β 1 through IL-1 β production. *J Oral Biosci*. 2020;62(1):44–51.
61. Bott KN, Feldman E, de Souza RJ, et al. Lipopolysaccharide-induced bone loss in rodent models: a systematic review and meta-analysis. *J Bone Miner Res*. 2023;38(1):198–213.
62. Guo C, Yuan L, Wang JG, et al. Lipopolysaccharide (LPS) induces the apoptosis and inhibits osteoblast differentiation through JNK pathway in MC3T3-E1 cells. *Inflammation*. 2014;37(2):621–631.

63. Bandow K, Maeda A, Kakimoto K, et al. Molecular mechanisms of the inhibitory effect of lipopolysaccharide (LPS) on osteoblast differentiation. *Biochem Biophys Res Commun*. 2010;402(4):755–761.
64. Mo IF, Yip KH, Chan WK, et al. Prolonged exposure to bacterial toxins downregulated expression of toll-like receptors in mesenchymal stromal cell-derived osteoprogenitors. *BMC Cell Biol*. 2008;9:52.
65. van den Berk LC, Jansen BJ, Siebers-Vermeulen KG, et al. Toll-like receptor triggering in cord blood mesenchymal stem cells. *J Cell Mol Med*. 2009;13(9b):3415–3426.
66. Albiero ML, Amorim BR, Martins L, et al. Exposure of periodontal ligament progenitor cells to lipopolysaccharide from *Escherichia coli* changes osteoblast differentiation pattern. *J Appl Oral Sci*. 2015; 23(2):145–152.
67. He X, Wang H, Jin T, et al. TLR4 activation promotes bone marrow MSC proliferation and osteogenic differentiation via Wnt3a and Wnt5a signaling. *PLoS One*. 2016;11(3):e0149876.
68. Sacchetti B, Funari A, Remoli C, et al. No identical "mesenchymal stem cells" at different times and sites: human committed progenitors of distinct origin and differentiation potential are incorporated as adventitial cells in microvessels. *Stem Cell Rep*. 2016;6(6):897–913.
69. Valido E, Bertolo A, Fränkl GP, et al. Systematic review of the changes in the microbiome following spinal cord injury: animal and human evidence. *Spinal Cord*. 2022;60(4):288–300.
70. Jogia T, Ruitenberg MJ. Traumatic spinal cord injury and the gut microbiota: current insights and future challenges. *Front Immunol*. 2020;11:704.
71. Nayfach S, Shi ZJ, Seshadri R, Pollard KS, Kyrpides NC. New insights from uncultivated genomes of the global human gut microbiome. *Nature*. 2019;568(7753):505–510.
72. Thefenne L, de Brier G, Leclerc T, et al. Two new risk factors for heterotopic ossification development after severe burns. *PLoS One*. 2017; 12(8):e0182303.
73. Orchard GR, Paratz JD, Blot S, Roberts JA. Risk factors in hospitalized patients with burn injuries for developing heterotopic ossification— a retrospective analysis. *J Burn Care Res*. 2015;36(4):465–470.
74. Evans KN, Forsberg JA, Potter BK, et al. Inflammatory cytokine and chemokine expression is associated with heterotopic ossification in high-energy penetrating war injuries. *J Orthop Trauma*. 2012; 26(11):e204–e213.
75. Manrique J, Alijanipour P, Heller S, Dove M, Parvizi J. Increased risk of heterotopic ossification following revision hip arthroplasty for periprosthetic joint infection. *Arch Bone Jt Surg*. 2018;6(6):486–491.
76. Rosteius T, Rausch V, Pätzholz S, et al. Incidence and risk factors for heterotopic ossification following periprosthetic joint infection of the hip. *Arch Orthop Trauma Surg*. 2019;139(9):1307–1314.
77. Scott BN, Roberts DJ, Robertson HL, et al. Incidence, prevalence, and occurrence rate of infection among adults hospitalized after traumatic brain injury: study protocol for a systematic review and meta-analysis. *Syst Rev*. 2013;2:68.
78. Helling TS, Evans LL, Fowler DL, Hays LV, Kennedy FR. Infectious complications in patients with severe head injury. *J Trauma*. 1988;28(11): 1575–1577.
79. Garcia-Arguello LY, O'Horo JC, Farrell A, et al. Infections in the spinal cord-injured population: a systematic review. *Spinal Cord*. 2017; 55(6):526–534.
80. Ferrucci JL, Sassi FC, Medeiros GC, Andrade CRF. Comparison between the functional aspects of swallowing and clinical markers in ICU patients with traumatic brain injury (TBI). *CoDAS*. 2019;31(2): e20170278.
81. Nakata H, Yamakawa K, Kabata D, et al. Identifying septic shock populations benefitting from polymyxin B hemoperfusion: a prospective cohort study incorporating a restricted cubic spline regression model. *Shock*. 2020;54(5):667–674.
82. Opal SM, Laterre P-F, Francois B, et al. Effect of eritoran, an antagonist of MD2-TLR4, on mortality in patients with severe sepsis: the ACCESS randomized trial. *JAMA*. 2013;309(11):1154–1162.
83. Rice TW, Wheeler AP, Bernard GR, et al. A randomized, double-blind, placebo-controlled trial of TAK-242 for the treatment of severe sepsis. *Crit Care Med*. 2010;38(8):1685–1694.